Geophys. J. R. astr. Soc. (1986) **87**, 79–116

Post-glacial rebound and transient lower mantle rheology

W. R. Peltier, R. A. Drummond and A. M. Tushingham

Department of Physics, University of Toronto, Toronto, Ontario M5S 1A7, Canada

Accepted 1986 April 4. Received 1986 March 3; in original form 1985 July 16

Summary. Although post-glacial rebound data have been conventionally interpreted as being governed by the steady state component of the mantle viscosity spectrum, the radial profile of this parameter, which is then inferred by fitting a model to observations, is characterized by the fact that it exhibits rather slight variation with depth. This disagrees with expectations based upon microphysical models of the solid state creep process. It also disagrees with very recent inferences of the viscosity stratification based on isostatic geoid anomalies expected on the basis of the internal lateral heterogeneity of mantle density obtained from seismic tomographic analyses. The new calculations of the signatures of post-glacial rebound reported here show that these two types of information are easily reconciled if the previously inferred value of the lower mantle viscosity is interpreted as a transient value, as originally suggested by Weertman on the basis of qualitative considerations. In these new models considered here the steady state creep resistance of the lower mantle is not constrained at all by post-glacial rebound observations. It can be fixed only by an appeal to other geophysical data. Whether such models are actually required by the data should become clear in the very near future.

Key words: post-glacial rebound, lower mantle viscosity, transcience

1 Introduction

In the past 10 years a rather large number of different geophysical observations have been successfuly interpreted as representing different signatures of the planet's response to the glaciation-deglaciation cycle which has dominated the last million years of Earth history. Although it has long been recognized that the raised marine shorelines found above present-day sea-level throughout the Canadian Arctic, and in Fennoscandia surrounding the Gulf of Bothnia, are a consequence of the rebound of the crust subsequent to glacial unloading, it has only recently proved possible to unambiguously relate a number of other observations to this common cause. These additional data include the negative free air gravity anomalies

which are found over the main centres of rebound, as well as certain irregularities of the Earth's rotation, including the non-tidal component of the acceleration of rotation rate, and the secular drift of the pole with respect to the surface geography upon which the most evident annual and Chandler wobbles are superimposed.

The demonstration of the intimate connection which exists between these diverse observations has been achieved through systematic application of the viscoelastic theory of glacial isostatic adjustment based upon the analysis of this problem in Peltier (1974). That paper was devoted to the derivation of the impulse response of a radially stratified model of the planet to surface load forcing. Peltier (1976, 1985b) showed how this Green's function could be constructed using a normal mode formalism, and Peltier & Andrews (1976) first applied the theory to compute approximate relative sea-level (RSL) histories which could be directly compared to observed shorelines whose emergence/submergence curves were controlled by ^{14}C dating. These initial calculations of RSL variations were based upon the assumption that the meltwater generated in deglaciation entered the global ocean uniformly. Farrell & Clark (1976) showed how this assumption could be relaxed and a simple gravitationally self-consistent calculation performed which could account correctly for the irregular distribution of meltwater among the ocean basins which is required to ensure that the surface of the ocean (the geoid) remains an equipotential surface at all times during and subsequent to the unloading event. The full theory was first applied by Clark, Farrell & Peltier (1978) and Peltier, Farrell & Clark (1978) in detailed comparisons with observed sea-level histories at a global array of stations. These analyses demonstrated that a large fraction of the observed variability of RSL over the age range 0–18 k BP could be reconciled with the rather simple model of Würm–Wisconsin deglaciation first tabulated in Peltier & Andrews (1976) and later refined in Wu & Peltier (1983), and an equally simple model of the radial viscoelastic structure of the planet. Extensive new calculations of RSL histories in the latter paper showed that the full gravitationally self-consistent theory was not particularly important in the near field of the ice sheets, except for times during the actual deglaciation event. In that paper a surface lithosphere was also included in the radial viscoelastic structure but no sensitivity tests were performed to determine the importance of its contribution to the relative sea-level response. The main result of these analyses was the demonstration, on the basis of extensive calculations of RSL variations for sites within the ice sheet margins, that the viscosity of the lower mantle had to be rather close to the viscosity of 10^{21} Pa s which characterizes the upper mantle region. Wu & Peltier (1983) also found that there were large and systematic misfits of the predicted and observed RSL histories at sites in the region immediately peripheral to the margin of the Laurentian ice sheet. In Peltier (1984a) these misfits where shown to be the consequence of employing a lithosphere in the model which was too thin. In terms of the model employed to invert the data, which had an elastic structure equal to that of 1066B (Gilbert & Dziewonski 1975), the observations were shown to imply a continental lithospheric thickness in excess of 200 km. A number of further observations have recently been shown to accord with predictions of this model, including some tide gauge observations of present-day emergence rate on the North American continent (Peltier 1985c).

In parallel with these analyses of the radial viscoelastic structure implied by post-glacial RSL variations, other geophysical data mentioned previously have also been considered. Peltier (1981) and Peltier & Wu (1982) first established that the observed free air gravity anomalies over the main centres of rebound were compatible with the same almost constant mantle viseosity model preferred by the sea-level data. These anomalies had previously been thought to require a very high value of the viscosity of the lower mantle as they were very much in excess of those predicted by the uniform viscosity and density models of Haskell

(1935, 1936), for example. Walcott (e.g. 1970) has often drawn attention to this apparent contradiction. In the new models of glacial isostatic adjustment, discussed in detail in Wu & Peltier (1983), the reason why large amplitude present-day free air anomalies are predicted in spite of their uniform mantle viscosities is associated with the fact that these models contain internal buoyancy which is assumed to act in association with the near discontinuities of density across the seismic discontinuities at 420 and 670 km depth in the mantle. Although it might be thought that such buoyancy is not consistent with the interpretation of these boundaries as equilibrium phase boundaries, Peltier (1985a) has pointed out, on the basis of calculations of O'Connell (1976) and Mareschal & Gangi (1977), that such boundaries would behave as non-adiabatic chemical boundaries to the extent that the phase transitions involved may be considered to be univariant, since material will then change phase in response to an increase of normal stress only on the time-scale of thermal diffusion which is long compared to the time-scale of 10^5 yr between successive interglacials.

The rotational response of the planet to ice sheet loading and unloading was first reconsidered in the recent literature by Nakiboglu & Lambeck (1980, 1981) and Sabadini & Peltier (1981). These authors both employed homogeneous viscoelastic models of the planet to compute the polar wander and acceleration of rotation expected due to ice sheet forcing and concluded that the existing observations of both these quantities were entirely explicable as effects due to this cause. Peltier (1982) and more recently Wu & Peltier (1984) and Peltier (1984a) demonstrated that there were serious errors of analysis committed in both these papers which rendered the basis of their conclusions erroneous. As Munk & Revelle (1952) were aware, a homogeneous viscoelastic model of the planet will support a wander of the rotation pole only at a time during which the surface load to which it is subject is actually changing. When the surface load ceases to vary, all polar wander will immediately stop. Peltier (1982) and Wu & Peltier (1984) demonstrated, however, that this property was not shared by models with radial stratification. When realistic radial stratification of the viscoelastic parameters is introduced into the model, then the symmetry which caused the polar wander to vanish for stationary surface loads was broken. This symmetry in the homogeneous model was shown to be due to the fact that for this model, but only for this model, the rotational and isostatic adjustment contributions to the rotational forcing precisely annihilate one another whenever the surface load is steady. When layering is introduced into the viscoelastic structure, cancellation no longer occurs and it becomes possible to explain the polar wander evident in the ILS path (e.g. Vincenti & Yumi 1969, 1970) as a memory of the planet of the cyclic glaciation-deglaciation process which ended about 7000 yr ago and since which continental ice sheets have remained in a steady state. As was the case with observed free air gravity anomalies, both rotational observables were shown to be compatible with the same radial viscoelastic structure as was required to explain relative sea-level observations.

The model which has been employed to fit all of these data is one based upon a simple linearly viscoelastic Maxwell representation of the rheology of the mantle. This rheology is such that when it is subject to an applied shear stress its instantaneous response is Hookean elastic while its final response is Newtonian viscous. The transition from initial elastic to final viscous behaviour takes place over a time-scale $T_M = \nu/\mu$ called the Maxwell time, where ν is the Newtonian viscosity and μ is the elastic shear modulus. As a consequence of the analyses cited above, the profile $\nu(r)$ has been shown to be rather uniform and to consist of an upper mantle segment over the depth range 120 km $\leqslant d \leqslant$ 670 in which the viscosity $\nu_{UM} \simeq 10^{21}$ Pa s and a lower mantle segment over the depth range 670 km $\leqslant d \leqslant$ 2800 km in which $\nu_{LM} \simeq 3 \times 10^{21}$ Pa s. Since ν is the steady state viscosity the implication of these

analyses is that the mantle convective circulation should be governed throughout its volume by a creep resistance of this value. Not only is this plausible, it may also be argued on the basis of boundary layer theory for convection at high Rayleigh number (Peltier 1980, 1981, 1984b, 1985a) that if the steady state creep resistance were substantially different from this value then it would not be possible to reconcile the observed properties of the plate tectonic process in terms of the thermal convection hypothesis. Nevertheless, there are good reasons to believe that the steady state creep resistance should increase somewhat as a function of depth. Sammis *et al.* (1977) and Ellsworth, Schubert & Sammis (1984) for example, have argued on the basis of oxygen ion packing systematics and other microphysical considerations that the increase of viscosity from the upper to the lower mantle should be at least by a factor of 5 and perhaps by as much as a factor of 10^2. Weertman (1978) suggested that the explanation of the discrepancy between the weak viscosity stratification required by post-glacial rebound data and the strong stratification suggested by rheological considerations could be simply that the lower mantle viscosity to which post-glacial rebound is sensitive is a transient viscosity rather than the steady state value.

Very recently, new analyses have been forthcoming which appear rather strongly to support the interpretation of Weertman (1978). Hager (1984) and Richards & Hager (1984) have made use of the new models of the internal lateral heterogeneity of mantle density which have been inferred by the application of seismic tomographic techniques (Dziewonski, Hager & O'Connell 1977; Masters *et al.* 1982; Dziewonski 1984; Woodhouse & Dziewonski 1984), to infer the isostatic geoid anomalies which should be associated with the internal density heterogeneity. A simple incompressible Newtonian viscous parameterization of the mantle was employed to invert the observed long wavelength geoid height data for the viscosity stratification. This analysis suggested that when the viscosity of the upper mantle was fixed to the value of 10^{21} Pa s preferred by post-glacial rebound and other observations, then the lower mantle value was required to be at least one order of magnitude higher and preferred models had the viscosity of the lower mantle as much as two orders of magnitude higher than the upper mantle value. Given that the observed lateral density heterogeneity is most probably that which drives the convective circulation itself (Peltier 1985a), which has a characteristic time-scale of order 10^8 yr, it seems clear that the response to such internal loads must be governed by the steady state viscosity. The lower mantle viscosity required by the rebound data would then have to be a transient value in accord with Weertman's (1978) suggestion. Although it may be somewhat premature to adopt this interpretation, particularly given the reanalyses of the long wavelength geoid height and internal lateral heterogeneity observations by Forte & Peltier (1986), it is nevertheless important to address the possible implications of these new data to the question of mantle viscosity stratification and in particular to the previous interpretations of this stratification which have been obtained from the analysis of glacial rebound data with the Maxwell model. This is the purpose of the present paper.

In the next section we provide a very brief review of the theory which has previously been developed to explain relative sea-level changes and other signatures of the response of the planet to Pleistocene deglaciation. This review will focus on the way in which the rheological equation of state enters the theory and will discuss the application of the simple three-dimensional Burger's body rheology first developed in Peltier, Wu & Yuen (1981) as a representation of material behaviour which contains both explicit transient and steady state components of the viscosity spectrum. This analogue will be employed to demonstrate the way in which a transient component of the viscosity spectrum could masquerade as a steady state component when the elastic defect associated with the transient is large. This will be shown to provide a very simple confirmation of the possible validity of Weertman's

(1978) conjecture discussed above. Following this brief discussion of theory, the new results which have been obtained are discussed in Sections 3 and 4.

Section 3 describes the constraints on lower mantle viscosity derived on the basis of the conventional Maxwell parameterization of the rheological structure. Several new points are made in this section concerning the internal buoyancy required to explain observed free air gravity anomalies, concerning the constraint on deep mantle viscosity delivered by US east coast RSL data and by $\dot{J}_2$ inferred on the basis of laser ranging to the *LAGEOS* satellite, and concerning the future prospect for obtaining new information on the rheological stratification using absolute g instruments to measure $\dot{g}$ over the centres of post-glacial rebound. These calculations all reconfirm previous results to the effect that in terms of this parameterization of the rheology the viscosity of the mantle must be very nearly uniform.

In Section 4 a sequence of calculations of the same signatures of post-glacial rebound are performed based upon the new Burger's body representation of the rheology. For purposes of illustration it is assumed that only the lower mantle possesses a strong transient component of its viscosity spectrum and the steady state value is fixed to a number which is two orders of magnitude higher than the upper mantle value of 10^{21} Pa s, which would be completely ruled out in the context of a Maxwell model but which seems to be preferred by Richards & Hager's (1984) recent analysis of geoid height data. It is then shown by explicit recalculation of all of the signatures of post-glacial rebound that the Burger's body model may be employed to fit the observations only if the elastic defect is very large, in which limit the Burger's body degenerates to a Maxwell body governed by a viscosity which is essentially equal to the transient value. Therefore all previous inferences of lower mantle viscosity based upon application of the Maxwell analogue may be simply reinterpreted, if necessary, as delivering measures of the transient rather than the steady state creep resistance.

In the concluding Section 5 we discuss some implications of these new ideas concerning the rheology of the mantle and discuss further observations which may serve as useful tests of them.

2 Linear viscoelastic field theories of glacial isostasy

Since all of the mathematical apparatus which will be employed here has been published previously, it will serve no purpose to reproduce the derivations of the results which we will employ. For such detailed accounts the interested reader is referred to the original articles. Recent and rather comprehensive discussions of the theory to be employed here will be found in Wu & Peltier (1982, 1983, 1984) and an extensive review is contained in Peltier (1982). The main point which will concern us is the issue of mantle rheology and in particular the form of the stress strain relation which should be employed in a linear viscoelastic field theory to describe post-glacial rebound phenomena. Of the myriad of such forms which are conceivable we will restrict consideration here to linear viscoelastic equations of state embodied in stress-strain relations of the form:

$$\sigma_{kl} = \lambda(s)\, e_{kk}\, \delta_{kl} + 2\mu(s)\, e_{kl}, \tag{1}$$

which is written in the domain of the Laplace transform variable (complex frequency) s. The parameters $\lambda(s)$ and $\mu(s)$ which appear in (1) are frequency-dependent moduli whose functional forms depend upon the nature of the viscoelastic material which (1) is intended to represent while σ_{kl} and e_{kl} are respectively the components of the stress and strain tensors.

Fig. 1 shows conventional 1-D spring and dashpot representations of materials whose

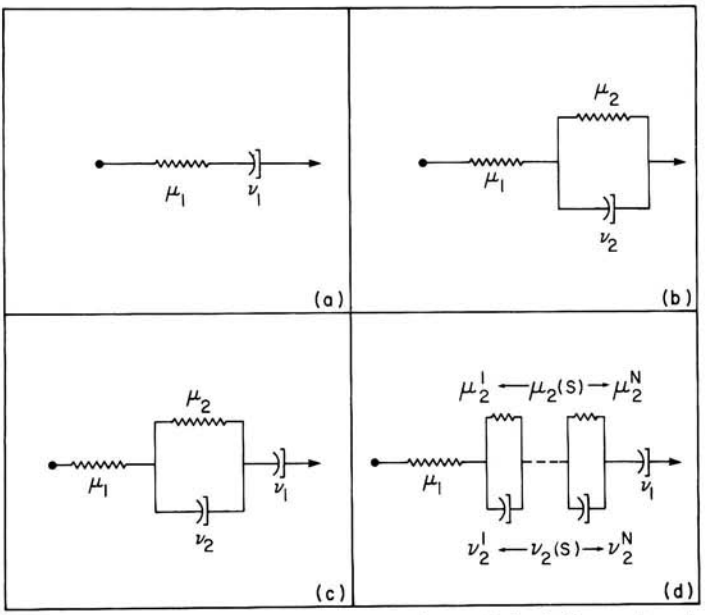

Figure 1. One-dimensional spring and dashpot analogues of several simple linear viscoelastic rheologies: (a) the Maxwell solid, (b) the standard linear solid, (c) the Burger's body solid, and (c) a generalized Burger's body solid with a (perhaps continuous) relaxation spectrum.

rheologies may be encompassed within the framework of equation (1). For the conventional Hookean elastic solid both λ and μ are frequency-independent while for the Maxwell solid illustrated in Fig. 1(a) the frequency-dependent modulii are (Peltier 1974):

$$\lambda(s) = \frac{\lambda_1 s + \mu_1 K/\nu_1}{s + \mu_1/\nu_1} \tag{2a}$$

$$\mu(s) = \frac{\mu_1 s}{s + \mu_1/\nu_1} \tag{2b}$$

in which $K = \lambda_1 + 2\mu_1/3$ is the elastic bulk modulus and λ_1 and μ_1 are the conventional Lamé parameters of Hookean elasticity. The Burger's body solid is illustrated by the analogy shown on Fig. 1(c) and in three spatial dimensions it has frequency-dependent moduli (Peltier *et al.* 1981):

$$\lambda(s) = \frac{(\lambda_1 s + \mu_1 K/\nu_1)(s + \mu_2/\nu_2) + \mu_1 K s/\nu_2}{(s + \mu_1/\nu_1)(s + \mu_2/\nu_2) + \mu_1 s/\nu_2}, \tag{3a}$$

$$\mu(s) = \frac{\mu_1 s}{s + \mu_1/\nu_1}\left[\frac{(s + \mu_2/\nu_2)(s + \mu_1/\nu_1)}{(s + \mu_2/\nu_2)(s + \mu_1/\nu_1) + \mu_1 s/\nu_2}\right] \tag{3b}$$

in each of which $K = \lambda_1 + 2\mu_1/3$ is the elastic bulk modulus as before and both solids have been designed to have zero bulk dissipation. Some previous application of the constitutive equation (3) has been made in Yuen & Peltier (1982) to the understanding of the Q's of the elastic gravitational normal modes of free oscillation. There it was shown that the very weak variation of Q with frequency which characterizes the free oscillations could not be reconciled by the single Debye peak representation of the anelastic relaxation which is

embodied in the Burger's body moduli (3). It was therefore suggested, following Peltier *et al.* (1981), that a more reasonable representation of the complete frequency dependence of the elastic moduli might be obtained by substituting a constant Q absorption band for the anelastic element of (3) (the terms in square brackets in 3b) to obtain the moduli:

$$\lambda(s) = K - \tfrac{2}{3}\mu(s) \tag{4a}$$

$$\mu(s) = \frac{\mu_1 s}{s + \mu_1/\nu_1}\left[1 + \frac{2}{\pi Q_m}\ln\left(\frac{s + T_2^{-1}}{s + T_1^{-1}}\right)\right], \tag{4b}$$

where T_1 and T_2 are the short-time and long-time cutoffs of the absorption band and where Q_m is the Q which is obtained within it. Yuen and Peltier (1982) showed that the model embodied in (4) very nicely reconciled the observed Q's of the elastic gravitational free oscillations with the choices $Q_m = 250$, $T_1 = 10^{-2}$ s and $T_2 = 10^4$ s of Minster (1978a, b). With these parameter values and the steady state viscosity $\nu_1 = \infty$ the above model has a very small elastic defect $\Delta = (\mu_1 - \mu_R)/\mu_R = 0.03$ where μ_1 is the initial elastic shear modulus and μ_R is its relaxed value. If the lower mantle viscosity which is felt by post-glacial rebound is to be a transient it is clearly not the same transient associated with the above described seismically required anelasticity. That embodied in (4) operates on far too short a time-scale and is characterized by far too small an elastic defect to accommodate the amount of relaxation necessary to reconcile post-glacial rebound data. If the additional transience which might be required by these data is representable as a single Debye peak such as is embodied in (3), this would imply the necessity of a new and more general rheology in the form:

$$\lambda(s) = K - \tfrac{2}{3}\mu(s) \tag{5a}$$

$$\mu(s) = \frac{\mu_1 s}{s + \mu_1/\nu_1}\left[\frac{(s + \mu_2/\nu_2)(s + \mu_1/\nu_1)}{(s + \mu_2/\nu_2)(s + \mu_1/\nu_1) + \mu_1 s/\nu_2}\right]\left[1 + \frac{2}{\pi Q_m}\ln\left(\frac{s + T_2^{-1}}{s + T_1^{-1}}\right)\right]. \tag{5b}$$

In the introduction to this paper we have cited some recent analyses which suggest that this extra transient peak in the relaxation spectrum is in fact required. In the remainder of this paper we will focus on an attempt to determine the values of the two new parameters μ_2 and ν_2 which determine its strength and the time-scale on which it operates. Since the high frequency elastic defect embodied in (4) is so small it will suffice for present purposes to suppose that the model embodied in equations (3) for the simple Burger's body will suffice to represent the combined effects of transient and steady state relaxation which are determined by the respective viscosities ν_2 and ν_1.

One property of this simple Burger's body rheology which will turn out to be particularly important for present purposes may be seen by considering the limit in which $\mu_2 \to 0$ so that the elastic defect $\Delta = \mu_1/\mu_2$ is large. In this limit the relaxed modulus $\mu_R = \mu_1\mu_2/(\mu_1 - \mu_2)$ of the standard linear solid part of the general constitutive relaxation is such that $\mu_R \to \mu_2$. In this limit, inspection of (3) shows that

$$\mu(s) \to \frac{\mu_1 s}{s + \mu_1(1/\nu_1 + 1/\nu_2)} = \frac{\mu_1 s}{s + \mu_1/\nu_{\text{eff}}}, \tag{6}$$

where

$$\nu_{\text{eff}} = \frac{\nu_1 \nu_2}{\nu_1 + \nu_2} . \tag{7}$$

This demonstrates that in a region of the Earth in which (3) is applicable, if $\mu_2 \ll \mu_1$ then the rheology is 'effectively' a Maxwell rheology (see equation 2) governed by the effective viscosity ν_{eff} defined in (7). If $\nu_2 \ll \nu_1$ then $\nu_{\text{eff}} \simeq \nu_2$ and where the Maxwell model is employed to infer the creep resistance the viscosity obtained will be the transient viscosity ν_2 rather than the steady state value ν_1. These are the conditions under which a transient viscosity ν_2 may 'masquerade' as a steady state value ν_1. One of the objects of this paper will be to determine how small μ_2 must be in order that the above asymptotic condition is reached and whether models for which it is not must be considered as possible candidates for the reconciliation of post-glacial rebound data. In order to investigate this point we will have to calculate the various signatures of glacial isostasy for models of this type and compare them with the observed signatures.

The calculations to be presented in this paper will all be based on the assumption that the ice sheets may be adequately approximated as circular disc loads applied to the surface of a radially stratified viscoelastic model of the planet. Several different earth models will be employed for the purpose of these calculations, including the simple homogeneous layer approximations to the actual structure of the planet whose properties are listed in Table 1, and the seismically realistic structures 1066B (Gilbert & Dziewonski 1975) and PREM (Dziewonski & Anderson 1981). The various signatures of the response which we will consider include relative sea-level histories, free air gravity anomalies, non-tidal acceleration of rotation and $\dot{J}_2$ observations, and the polar wander forced by ice sheet loading and unloading. We will also make predictions, based on the free air gravity calculations, of the time derivative of $g(\dot{g})$ which should soon be observable over the centres of rebound using new absolute g instruments (e.g. Zumberge, Rinkler & Faller 1982; Zumberge, Faller & Gschwind 1983). The mathematical forms which the predictions of each of these components of the response take are discussed in the following brief subsections.

2.1 RELATIVE SEA-LEVEL HISTORIES

As demonstrated explicitly in Wu & Peltier (1983), observations of post-glacial relative sea-level change in the near field of an ice sheet for times subsequent to the completion of melting are rather accurately approximated by the local variation of the radius of the solid earth since the geoidal surface then becomes almost stationary. The variation of radius forced by the disintegration of a circular ice cap may be represented by convolution of the Green's function for radial displacement (Peltier 1974) with the surface load. The radial displacement Green's function has the form:

$$G(\theta, t) = G_{\text{u}}^{\text{E}}(\theta)\,\delta(t) + \frac{a}{m_{\text{e}}} \sum_{n=0}^{\infty} h_n^{\nu}(t)\, P_n(\cos\theta), \tag{8}$$

where h_n^{ν} is the viscous part of the surface load Love number (Peltier 1974) of degree n for radial displacement which has the normal mode expansion:

$$h_n^{\nu}(t) = \sum_{j=1}^{M} r_j^n \exp(-s_j^n t), \tag{9}$$

where $s_j^n (j = 1, M)$ is the spectrum of inverse relaxation times required to synthesize the

Table 1. Parameter values for the earth models.

Model (per cent)	Structure	0–420 km	420–670 km	670–2900 km	Below 2900 K
0	Density	4 372	4 372	4 372	
	Percentage discontinuity	0	0		
	P velocity	11 013	11 013	11 013	
	S velocity	6 117	6 117	6 117	
6.2	Density	4 100	4 100	4 372	Modified 1066B
	Percentage discontinuity	0	6.2		
	P velocity	9 945	9 945	11 013	Core structure
	S velocity	5 475	5 475	6 117	
12.4	Density	3 828	3 828	4 372	$\rho = \rho_{1066B} - 1191$
	Percentage discontinuity	0	12.4		
	P velocity	8 877	8 877	11 013	$\text{pvel} = \text{pvel}_{1066B} - 2657$
	S velocity				$\text{svel} = \text{svel}_{1066B}$
6.2/3.8	Density	3 959	4 100	4 372	
	Percentage discontinuity	3.8	6.2		$g = g_{1066B} \frac{\rho}{\rho_{1066B}}$
	P velocity	9 323	9 945	11 013	
	S velocity	5 219	5 475	6 117	

Units: density, kg m^{-3}, velocity, m s^{-1}.

relaxation of the degree n component of the deformation spectrum, $r_j^n (j = 1, M)$ are the associated amplitudes of these modes for point mass forcing, a is the Earth's radius, and m_e is the Earth's mass. The function $G_u^E(\theta)$ is the elastic part of the Green's function and is determined entirely by the elastic structure $\lambda_1(r), \mu_1(r)$, and $\rho(r)$, where λ_1 and μ_1 are the usual elastic Lamé parameters and ρ is the density field. Since these parameters are determined by seismology all variations in the viscoelastic earth structure are embedded in the inverse relaxation time spectra s_j^n and the associated amplitude spectra r_j^n. No matter which of the rheologies (2)–(6) we might care to employ, their properties are collapsed into the structure of sets s_j^n and r_j^n for all purposes which will be of interest to us here. If the surface load is $L(\theta, t)$ then the radial response at time t is just:

$$u(\theta, t) = \int_{-\infty}^{t} G_u(t - t') * L(t')\, dt' \tag{10}$$

where $*$ indicates the spatial part of the convolution operation. Wu & Peltier (1982) provide explicit formulae for the evaluation of (10) in the case of disc loads with arbitrary profiles of height versus radius and these will be employed for the computations to be described here. In discussing both sea-level and other responses to the melting of the Laurentian, Fennoscandian, and Antarctic ice sheets we will make use of the properties of these ice masses listed in Table 2. As discussed in Peltier (1982), whenever the history of glaciation

Table 2. Ice sheet parameters.

	Laurentian	Fennoscandian	Antarctic
Mass M_i (kg) ($\times 10^{19}$)	2	0.56	0.70
Radius α_i (°)	15	9.5	20
Colatitude θ_i (°)	30	25.5	180
East longitude ϕ_i (°)	270	25.0	–

and deglaciation prior to ice sheet melting is required we will invoke the $\delta^{18}0$ data from deep sea sedimentary cores to constrain this history. These data demonstrate that for the past 800 000 yr the major ice sheets have appeared and disappeared in a highly periodic fashion with a period of 10^5 yr separating successive interglacials. Each pulse of glaciation has been characterized by a slow buildup over a period of about 9×10^4 yr and a fast collapse lasting 10^4 yr. A theory explaining the occurrence of this 'ice age cycle' has been developed in Peltier (1982), Peltier & Hyde (1984) and Hyde & Peltier (1985) to which the interested reader is referred for details. Here we will simply continue to approximate this glacial cycle by one or the other of the simple approximations shown in Fig. 2 whenever the assumption of initial equilibrium is not liable to be accurate. This assumption is least accurate in so far as the prediction of free air gravity anomalies is concerned.

2.2 FREE AIR GRAVITY ANOMALIES

The computation of free air anomalies proceeds in precisely the same way as the computation of RSL histories. The only difference in fact is in the Green's function employed in the convolution integral. This is such that the expression which replaces (8) is

$$G_g(\theta, t) = G_g^E(\theta)\,\delta(t) + \frac{ag}{m_e} \sum_{n=0}^{\infty} [2h_n^v(t) - (n+1)k_n^v(t)]\, P_n(\cos\theta) \tag{11}$$

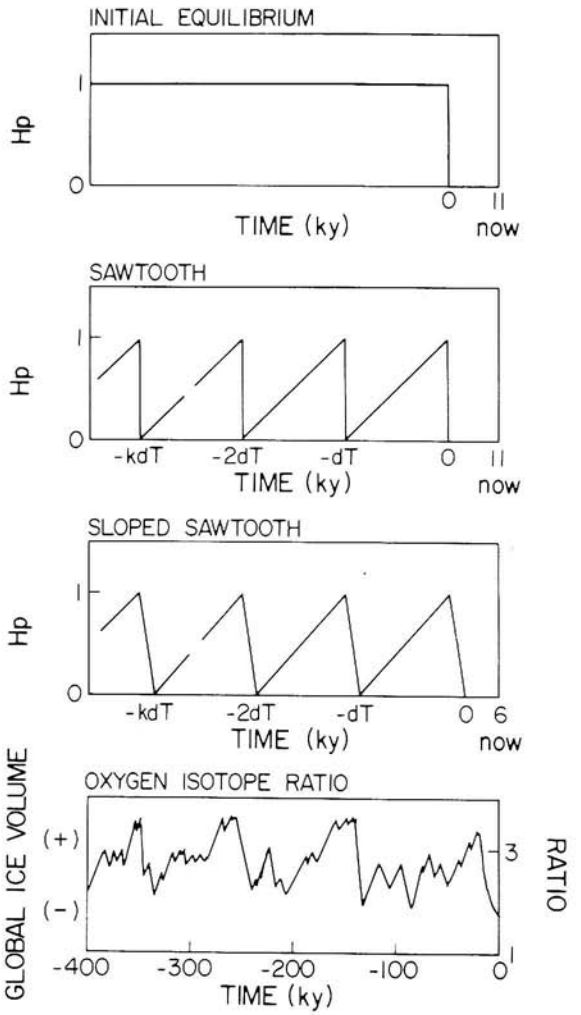

Figure 2. Simple approximations to the glaciation history. The best constraint on the history of continental ice volume fluctuations is provided by $\delta^{18}0$ data from deep sea sedimentary cores, one example of which is provided in the lowest trace. For all of the calculations in this paper we will employ the triangular sawtooth approximation to this history which has a period of 10^5 yr in which slow linear buildup of the individual ice sheet occurs on a time-scale of 9×10^4 yr followed by a fast collapse lasting 10^4 yr.

in which k_n^v is the viscous part of the surface load Love number for the perturbation of the gravitational potential. This Love number has a normal mode expansion which is entirely analogous to (9) in which the spectrum s_j^n is identical for the same earth model, but the amplitudes are different. In (11) the h_n Love number describes the contribution to the free air anomaly on the deformed surface due to the surface deformation itself, whereas the Love number k_n describes the contribution to the anomaly due to the internal redistribution of mass associated with the internal displacement field. To predict a free air anomaly we simply compute

$$\Delta g(\theta, t) = \int_{-\infty}^{t} G_g(t - t') * L(t')\, dt'. \tag{12}$$

The reason why this prediction is so much more sensitive to the history of ice loading and unloading prior to the last glacial maximum than is the radial displacement, has to do with the nature of the measurements to which these predictions are to be fitted. The RSL data are essentially measures of the history of radial displacement which has occurred at a given site during an interval of time up to the present day and the measure is taken relative to a present-day datum of zero displacement. RSL data therefore look backwards from the present into the past. They are therefore most sensitive to the shortest relaxation times which occur in the relaxation spectrum ($s_j^n, j = 1, M$). Free air gravity observations, on the other hand, are absolute measures of the currently existing degree of isostatic disequilibrium since they see the amount of relaxation which has yet to take place before equilibrium will be restored. These data therefore look forward into the future and are extremely sensitive to the longest relaxation times which may exist in the spectrum s_j^n ($j = 1, M$). For an ice age cycle of characteristic time-scale 10^5 yr, modes with relaxation times very much shorter than this will be in equilibrium by glacial maximum but modes with longer relaxation times will not. It turns out, as we will further demonstrate here, that the modes of relaxation which may be supported by internal density discontinuities in the mantle have relaxation times considerably in excess of 10^5 yr and therefore we must take careful account of the entire load history in order to compute their effect on the free air gravity anomaly predictions accurately.

2.3 THE NON-TIDAL ACCELERATION OF PLANETARY ROTATION AND $\dot{J}_2$

Given the enormous mass and extent of the ice loads which existed on the Earth's surface at glacial maximum 18 000 yr ago, it should not be too surprising that their melting induced rather large changes in the elements of the moment of inertia tensor of the planet and thus caused very substantial changes in the Earth's rotation. In fact these rotation effects induced by the last unloading event of the glacial cycle are continuing even today, almost 7000 yr after deglaciation was complete. The first of the rotation effects which we will be analysing in the next section consists of the so-called non-tidal component of the acceleration of rotation which was first inferred to exist by the analysis of ancient eclipse data (e.g. Müller & Stephenson 1975) but which has been reconfirmed through analysis of laser ranging data to the *LAGEOS* satellite which deliver a measure of $\dot{J}_2$, the time derivative of the degree two axial component of the Earth's gravitational potential field. Dicke (1966) was the first to suggest that this anomaly in planetary rotation might be caused by deglaciation. There is a simple 1:1 relation between the value of $\dot{J}_2$ and that of the non-tidal acceleration $(\dot{\omega}_3/\omega)_{\mathrm{NT}}$ which can be employed to demonstrate the consistency of the two data. Two different estimates of $\dot{J}_2$ have been inferred from the *LAGEOS* data, one by Yoder *et al.* (1983) has the value $\dot{J}_2 = -(7.0 \pm 0.6) \times 10^{-11}$ yr^{-1} while the other by Rubincam (1984) has the value $\dot{J}_2 = -(5.2 \pm 1.1) \times 10^{-11}$ yr^{-1}. Since it is not known why these two numbers differ to the extent they do we will consider the different implications of both. The estimate of Yoder *et al.* is closer to that previously based on eclipse data (e.g. Lambeck 1980). As shown in Peltier (1982) the non-tidal acceleration prediction takes the form:

$$(\dot{\omega}_3/\omega)_{\mathrm{NT}} = -\frac{I_{33}^{\mathrm{R}}}{C}\left[D_1 \dot{f}(t) + \sum_j r_j \frac{d}{dt}\left[f * \exp(-s_j t)\right]\right]$$

$$= -\dot{J}_2 \cdot 2m_e a^2/3C, \tag{13}$$

where C is the unperturbed axial component of the Earth's inertia tensor, I_{33}^{R} is the

maximum perturbation of this component which would be produced by accreting all of the major ice sheets from oceans of realistic shape if the Earth were rigid, $D_1 = 1 + k_2^{LE}$ where k_2^{LE} is the elastic part of the Love number for the gravitational potential perturbation of degree 2, $f(t)$ is one of the load history functions shown in Fig. 2, s_j and r_j are the inverse relaxation time and amplitude spectra associated with k_2^{ν} and * indicates convolution in time. Table 3 lists the perturbations to all of the important elements of the inertia tensor which would be produced by accreting the ice sheets with properties listed in Table 2 from realistic oceans on a rigid earth. Again all of the radial viscoelastic structure of the planet is embedded in the spectra $(s_j, r_j), j = 1, M$ irrespective of which of the rheologies (2)–(5) is employed to characterize this structure.

Table 3. Inertial perturbations I_{13}^{R} with realistic oceans and direction of polar wander θ.

	I_{13}^{R} (kg m^2)	I_{23}^{R} (kg m^2)	I_{33}^{R} ($\times 10^{32}$)	θ
Laurentia only (L)	1.203×10^{31}	3.491×10^{32}	-3.420	$-91°.97$
Fennoscandia only (F)	-7.504×10^{31}	-3.227×10^{31}	-1.130	$23°.27$
Antarctica only (A)	4.211×10^{30}	5.370×10^{30}	-1.799	$-128°.10$
L + F	-6.301×10^{31}	3.168×10^{32}	-4.550	$-78°.75$
L + F + A extra	-5.880×10^{31}	3.222×10^{32}	-6.349	$-79°.60$

2.4 LONG TIME-SCALE POLAR WANDER INDUCED BY THE GLACIATION CYCLE

Just as the rate of the Earth's rotation is caused to change by the variation of the axial component of the inertia tensor forced by glaciation and deglaciation, so perturbations of the off-diagonal elements of this tensor cause the position of the pole to wander with respect to the surface geography. The first correct theory for the prediction of this effect for radially stratified models of the planet was that in Peltier (1982) and Wu & Peltier (1984). The mathematical form which this prediction takes is considerably more complicated than that for the non-tidal acceleration given in (13), a consequence of the fact mentioned in the introduction that the mechanics of this process are such that for a homogeneous model of the planet the polar wander vanishes when the surface load is steady. Inspection of (13) shows that this is not the case for the non-tidal acceleration, since the presence of the convolution integral ensures that even in the 1 mode case ($M = 1$) which obtains for the homogeneous model, at a time when $\dot{f} = 0$ (the surface load is steady), $(\dot{\omega}/\omega)_{NT} \neq 0$, in general. The mathematical form of the prediction for the speed of polar wander, on the other hand, is:

$$(\omega_j/\omega) = \frac{\Omega}{A\sigma_0} \left[\left[D_1 \dot{f}(t) + D_2 f(t) + \sum_{i=1}^{M-1} E_i \frac{d}{dt} [f * \exp(-\lambda_i t)] \right]\right] \tag{14}$$

where

$$D_1 = 1 + k_2^{LE} \tag{15a}$$

$$D_2 = -\frac{l_s q(0)}{\prod_{i=1}^{M-1} \lambda_i} \tag{15b}$$

$$E_i = \left[\frac{l_s q(-\lambda_i)}{\lambda_i} + \sum_{j=1}^{M} \frac{r_j R_j(-\lambda_i)}{s_j} \right] \Big/ \prod_{k \neq i}^{M-1} (\lambda_k - \lambda_i) \tag{15c}$$

in which $I_s = \lim(s \to 0)\,[1 + k_2^L(s)]$ is the so-called isostatic factor (Munk & McDonald 1960), and the λ_i are the roots of the degree $M-1$ polynomial

$$Q_{M-1} = \sum_j g_j \left[\prod_{i \neq j} (s + s_i)\right] = \prod_{i=1}^{M-1} (s + \lambda_i) \tag{16}$$

in which the numbers g_j are the relative strengths of the M modes which are required to represent the viscous part of the tidal Love number of degree 2 (see Peltier 1982 and Wu & Peltier 1984). The functions q and R_j are defined as:

$$q(s) = s \prod_{i=1}^{M-1} (s + \lambda_i) - \prod_{i=1}^{M} (s + s_i) \tag{17}$$

$$R_j(s) = \prod_{i=1}^{M-1} (s + \lambda_i) - \prod_{i \neq j} (s + s_i). \tag{18}$$

In the limit that the earth model becomes homogeneous the number of modes tends to one ($M = 1$) and the third term in the solution (14) vanishes. Since this term is the only one which contains a history dependence (i.e. has the form of a convolution integral) it is clear that for a homogeneous earth model with $M = 1$, whenever $f = \dot{f} = 0$ there will be no polar wander. Since we are currently (apparently) at such a time of hiatus in a previously continuous 10^5 yr periodic glacial cycle, we are obviously obliged to rely on the non-vanishing of the last term in (14) to explain the observed polar wander in the ILS path at a rate near $(0.95 \pm 0.15)^\circ$ per 10^6 yr towards Hudson Bay which is occurring today. This term will differ from zero only to the extent that the planet is radially stratified. The polar wander datum is therefore particularly sensitive to this stratification as we will further verify here (see Wu & Peltier 1984 and Peltier 1984a, b for further recent discussions).

In the following sections we will proceed to employ the theoretical structures outlined above to investigate the nature of the constraints on the radial viscoelastic stratification which are imposed by the four characteristically different geodynamic observables.

3 Results based upon the conventional Maxwell parameterization

Even if a transient component of the lower mantle viscosity spectrum should be required to reconcile post-glacial rebound observations and geoid height anomalies associated with the mantle convection process, the previous discussion of alternate linear viscoelastic representations of the rheology demonstrates that under certain conditions a Maxwell analogue may nevertheless be appropriate. To the extent that the transient component of the relaxation may be represented in terms of the single Debye peak of the Burger's body, it is clear from the preceding analysis that if the elastic defect associated with this transient is sufficiently large then the Burger's body will behave as a Maxwell body with the effective viscosity $\nu_{\rm eff} = \nu_1 \nu_2 / (\nu_1 + \nu_2)$, where ν_1 is the steady state and ν_2 the transient viscosity as before. Clearly then if $\nu_1 = \nu_2$, $\nu_{\rm eff} = \nu_1/2$, whereas if $\nu_1 \gg \nu_2$ then $\nu_{\rm eff} \simeq \nu_2$. Models with large defects may therefore behave as Maxwell solids with a viscosity close to the steady state viscosity or with a viscosity (the transient viscosity ν_2) which may be infinitely distant from the steady state value. One of the most important points to be made in this paper is that it is only if the elastic defect associated with the transient component of the relaxation is very large (i.e. $\mu_2/\mu_1 \ll 1$), in which case the solid looks like a Maxwell solid, that this model is a plausible one in so far as the phenomena of glacial isostasy are concerned. In order to demonstrate this fact we will first review and extend previous analyses based upon

the Maxwell analogue in order to focus attention upon the type of observations which I have previously invoked to constrain the radial structure. This discussion will be provided in the following subsections. In Section 4 the same data will be addressed in terms of the Burger's body analogy and employed to demonstrate the validity of the above assertion.

3.1 RELATIVE SEA-LEVEL CONSTRAINTS ON THE RADIAL STRUCTURE OF THE MAXWELL MODEL

In both this and the following section of the present paper, all of the analyses described will be based upon circular parabolic disc load representations of the major ice sheets and RSL data will be approximated by the radial displacement response at sites located an appropriate distance from the centre of the equivalent disc load. The actual locations to which our analyses will be applied are shown on the location maps in Wu & Peltier (1983) (Figs 12 and 13) and are listed in Table 4 along with their distances from the centre of the model

Table 4. Distance of 'typical' stations from the centre of the Laurentian ice sheet.

Area	Station	Distance (degrees)
Near centre	Southampton Islands	1.2
	Churchill	1.5
	Ottawa Islands	2.3
Just inside the margin	NW Newfoundland	13.0
At the margin	Prince Edward Islands	15.0
	Bay of Fundy	15.0
	Maine	15.0
	New Hampshire	15.0
	Boston	15.0
	Clinton Conn.	15.0
Just outside the margin	Brigantine NJ	18.0
Far beyond the margin	Florida	28.0

Laurentian disc load which has a radius of 15°, and whose other properties are listed in Table 2. The recent analyses in Peltier (1984a, b) suffice to demonstrate that in so far as RSL data at sites near the ice sheets are concerned, the load may be assumed to be in isostatic equilibrium prior to the time disintegration commences. We will nevertheless employ the 'sloped-sawtooth' approximation to the load history shown in Fig. 2 for all calculations in order to include the small effects on the predictions due to isostatic disequilibrium prior to the commencement of melting.

In our analyses we will use the sequence of model elastic structures whose properties were previously listed in Table 1. Coupled with a model of the radial variation of viscosity, this structure suffices to determine the relaxation spectra s_j^n $(j = 1, M)$ and the amplitude spectra r_j^n $(j = 1, M)$ which are required to make any of the theoretical predictions discussed in the last section (RSLs, free air gravity anomalies, non-tidal acceleration of rotation, true polar wander). It should be noted, however, that although the relaxation spectrum is a unique property of the viscoelastic structure, two different amplitude spectra are required for these calculations, one for the Love number h_n and one for the Love number k_n. We will begin our presentation of the results of the radial displacement (relative sea-level) calculations by

first describing a sequence of relaxation time and amplitude spectra for some of the models listed in Table 1. The relaxation time and amplitude spectra will be represented respectively by $\log_{10}(-s_n^j)$ and $\log_{10}(-r_j^n/s_j^n)$ as a function of spherical harmonic degree n (marked L on the figures). We have not previously employed amplitude spectra plotted in this way but, as we will show, they do provide a very effective way of representing this extra dimension of the relaxation process.

Figs 3 and 4 illustrate the effect on the relaxation time and amplitude spectra of the presence of increasing amounts of internal buoyancy in the mantle. The first set of results in Fig. 3 (top) are for the model with no internal mantle buoyancy which is seen to possess only three different modes of relaxation at each spherical harmonic degree, labelled respectively MO, LO, CO. According to the nomenclature of Peltier (1976) these are the fundamental modes of the mantle, lithosphere, and core which owe their existence respectively to the density jump across the free outer surface of the model, to the assumed infinite contrast of viscosity between the lithosphere and the mantle, and to the large density jump across the core–mantle boundary. Note that time has been non-dimensionalized with a characteristic time of 10^3 yr so that $\log_{10}(-s) = -1$ corresponds to a relaxation time s^{-1} of 10^4 yr. In Figs 3–8 the lithospheric thickness is fixed at 120 km, the upper mantle viscosity to 10^{21} Pa s, and the lower mantle viscosity to 7×10^{21} Pa s for purposes of illustration. As discussed in Peltier (1976) and related articles, the trend to increasing relaxation time with increasing wavenumber (spherical harmonic degree) in the fundamental mode MO which is obtained at small degrees is reversed for degrees beyond 10, a consequence of the presence of the lithosphere. The relaxation time of the mode CO generally increases monotonically with degree. Inspection of Fig. 3(b) for the variation of modal amplitude demonstrates that the fundamental mode MO is dominant at all L and that the core mode contributes significantly to the relaxation only for degree L less than about 8, which is not surprising since only the longest deformation wavelengths 'see' to the depth of the CMB. The LO mode is only weakly excited in this model. Although we will not have occasion to discuss them here, higher modes of the lithosphere branch (L1, L2, ... etc.) exist when the transition from relatively low viscosity in the mantle to essentially infinite viscosity in the lithosphere takes place over a finite rather than an infinitesimal range of depths. The extra relaxation from these higher modes has been shown to be important in understanding the dynamics of sedimentary basins (e.g. Courtney 1982; Quinlan & Beaumont 1984; Wolf 1985) and would doubtless be equally important for other dynamical phenomena of similar temporal and spatial scale. In Figs 3–8 we have also suppressed the set of transition modes whose relaxation times are close to the Maxwell time since the amplitudes of these modes are very small.

Fig. 4 provides analogous relaxation time and modal amplitude data for a model which is identical to that discussed above except that it contains an internal density jump in the mantle at 670 km depth across which the density increases by 6.2 per cent (see Table 1 for parameter listing). The net effect of the introduction of this feature into the model is the appearance of the new family of modes which comprise the M1 branch, along which relaxation times are of order 10^6 yr; that is, considerably longer than those belonging to the other branches of the modal diagram. Peltier & Wu (1982), Peltier (1982) and Wu & Peltier (1983) first drew attention to the possibility that this mode may be required to understand the free air gravity anomalies observed over regions of post-glacial rebound which are otherwise too large to be reconciled with the almost uniform mantle viscosity which is required by relative sea-level observations. The remaining figures in this sequence, (5–8), respectively, show results for a model with a density increase of 12.4 per cent at 670 km depth, for a model with a density increase of 6.2 per cent at 670 km and a density increase of 3.8 per

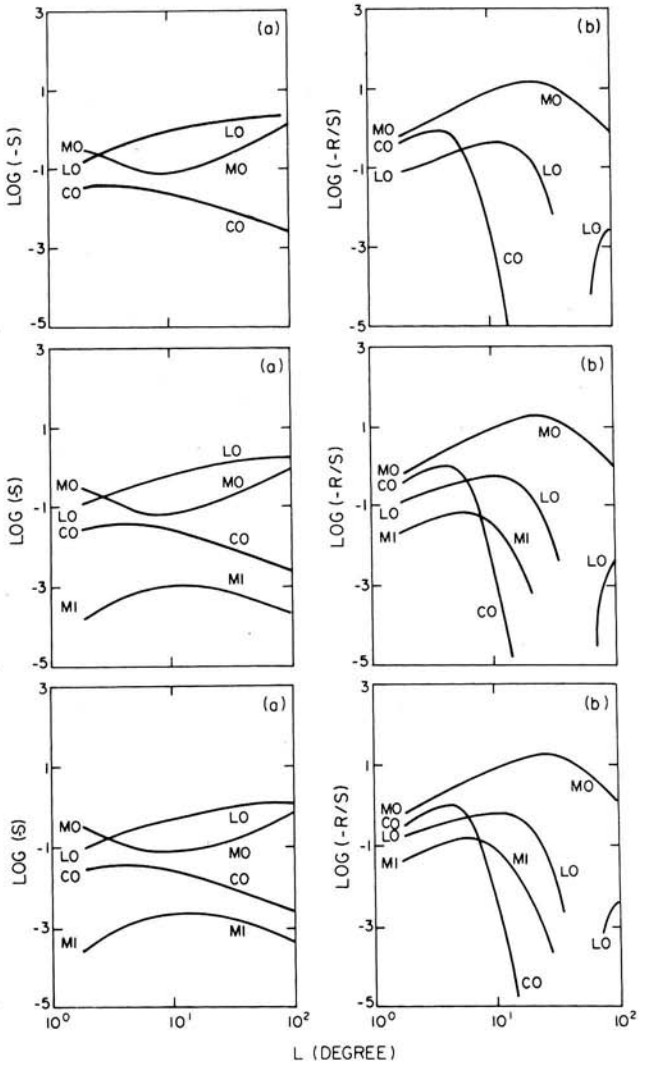

Figure 3.

Figure 4.

Figure 5.

Figure 3. (Top) Relaxation time (a) and amplitude spectra (b) for the Maxwell earth model in Table 1 which has no internal buoyancy within the mantle (the 0 per cent model). The individual modal branches consist of the fundamental mantle (MO) supported by the density jump across the free outer surface of the model, the lithosphere mode (LO) supported by the infinite contrast in viscosity across the mantle–lithosphere interface, and the core mode (CO) supported by the large density discontinuity across the CMB.

Figure 4. (Middle) Same as Fig. 3 but for a model with a single density discontinuity at 670 depth in the mantle. This supports the new mode M1.

Figure 5. (Bottom) Same as Fig. 3 but for a model which has an enhanced density discontinuity at 670 km depth in the mantle of 12.4 per cent rather than the 6.2 per cent in Fig. 4. This reduces the relaxation time of the M1 mode and increases its strength for all L.

cent at 420 km, for the seismically realistic model 1066B (Gilbert & Dziewonski 1975), and for the seismically realistic model PREM (Dziewonski & Anderson 1981). The effect of the introduction of the second discontinuity at 420 km depth (Fig. 6) is the appearance of the new modal family M2 along which relaxation times are even longer than those of the M1 models. Comparing the Figs 6–8 it is clear that there are only relatively minor differences

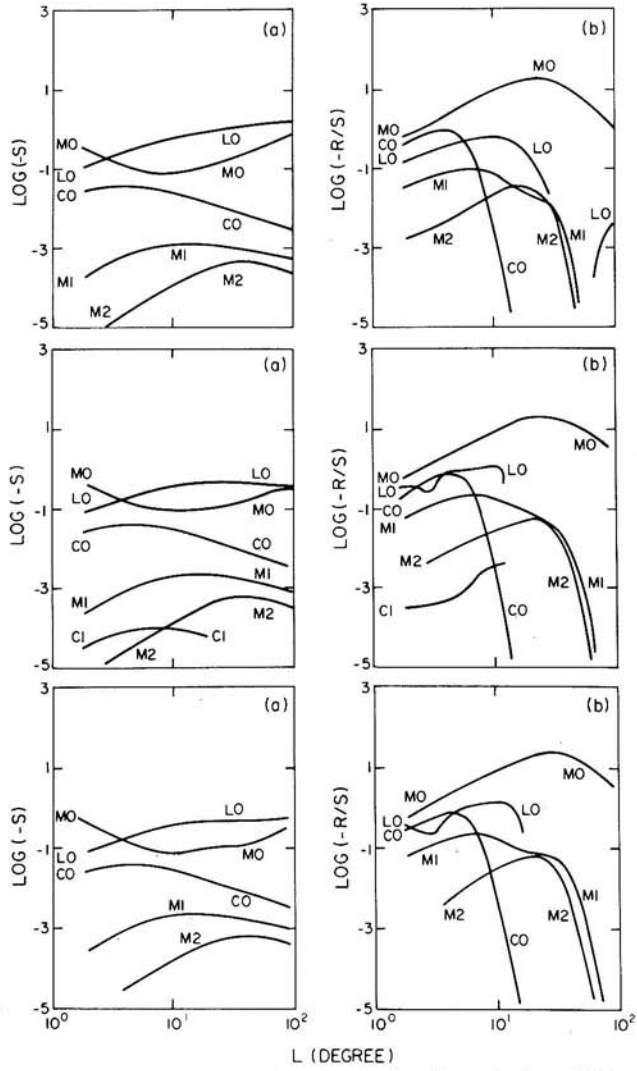

Figure 6.

Figure 7.

Figure 8.

Figure 6. (Top) Same as Fig. 3 but for a model which has a density discontinuity of 6.2 per cent at 670 km depth and 3.8 per cent at 420 km depth. The latter discontinuity introduces the new modal branch M2 into the spectra.

Figure 7. (Middle) Same as Fig. 3 but for the seismically realistic model 1066B of Gilbert & Dziewonski (1975).

Figure 8. (Bottom) Same as Fig. 3 but for the seismically realistic model PREM of Dziewonski & Anderson (1981).

between the homogeneous layered model with two internal discontinuities and either of the seismic models 1066B or PREM. It is evident from comparing these three models that the LO and CO modes interact more strongly in the seismically realistic models than they do in the layered approximation to them. In addition to the dominant modes discussed here the continuously stratified models 1066B and PREM also support an infinite sequence of modes which have extremely long relaxation times and very small amplitudes which are supported by the non-zero buoyancy which is associated with the slow increase of density with depth in the Earth which exists as a consequence of the adiabatic compression of mantle material

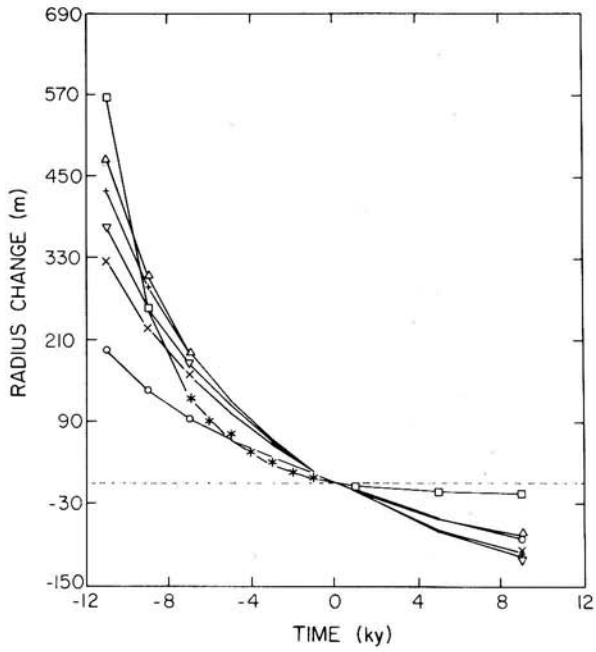

Figure 9. Predicted RSL histories at Churchill based upon Maxwell models whose lower mantle viscosities are respectively 10^{21} Pa s (□), 3×10^{21} Pa s (Δ), 5×10^{21} Pa s (+), 7×10^{21} Pa s (∇), 10^{22} Pa s (x) and 5×10^{22} Pa s (0). In all calculations the upper mantle viscosity is fixed to 10^{21} Pa s and the lithospheric thickness to 120.7 km. The elastic basic state employed is that with 3.8 and 6.2 per cent density discontinuities at 420 and 670 km depths respectively and the sea-level predictions are approximated by the radial displacement response.

under its own weight. Since this component of the stratification *is* adiabatic it should not contribute any buoyancy to the mantle interior. It does so in the present models only because they are implicitly isothermal. The gradient of the density profile between the major mantle discontinuities is so slight, however, that the modal structure of the realistic models is very close indeed to the modal structure of an appropriate homogeneous layer approximation to them.

As a first illustration of the application of these Maxwell viscoelastic models of the rheology to the explanation of RSL data we show in Fig. 9 a sequence of predicted RSL curves for the Churchill site which is assumed, according to the location information in Table 4, to be located 1.5° from the centre of the model Laurentian ice sheet. The observed variation of RSL at this site is denoted by the stars and theoretical results are shown for models which all have lithospheric thicknesses of 120 km, upper mantle viscosities of 10^{21} Pa s, and are based upon the elastic structure which has a 3.8 per cent density increase at 420 km depth and a 6.2 per cent density increase at 670 km depth. Calculations are shown for models whose lower mantle viscosities are respectively, 1x, 3x, 5x, 7x, 10x and 50x the upper mantle value of 10^{21} Pa s. These comparisons clearly demonstrate the point made in previous such analyses that the uniform viscosity model provides by far the best fit to the observations. Increasing the lower mantle viscosity by even a relatively small factor causes the theory to predict far too great a rate of present-day emergence, while increasing the lower mantle viscosity even further to correct this misfit to present-day emergence rates (i.e. x50) than leads to increasingly large misfits to the amplitude of emergence of the 7000 yr old beach. The complementary nature of the present-day emergence rate and early

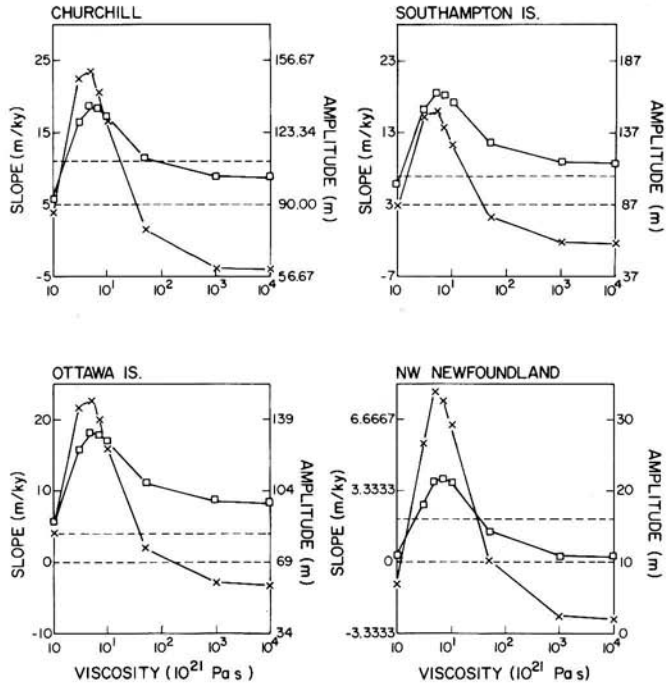

Figure 10. Comparisons of the predicted height of the 7 k BP beach and the present-day emergence rate with the observations at four sites within the margin of the Laurentian ice sheet. The predictions are shown as a function of lower mantle viscosity in the Maxwell parameterization and the elastic basic state is the same as that which was employed to construct Fig. 9. Note that only the homogeneous model (upper mantle viscosity is fixed to the value of 10^{21} Pa s) provides a satisfactory fit to both these data at all sites.

emergence amplitude observations at interior sites is demonstrated very clearly by Fig. 10 on which these two observations at each of four interior sites are collapsed onto a single allowed region between the horizontal dashed lines. The predictions of these two observations at each of the four sites are then shown as a function of lower mantle viscosity with the upper mantle value fixed at 10^{21} Pa s. This figure makes clear the fact that only the uniform viscosity model, in the context of the Maxwell parameterization, is able to reconcile both observations for the same choice of lower mantle viscosity.

Previous analyses of the sea-level variations forced by ice sheet disintegration have established that observations from outside the ice margin are equally important in constraining the magnitude of the viscosity contrast between the upper and lower mantles. One feature of the observations in this region which is particularly important in this regard concerns the characteristic variation of sea-level at sites which are located very close to the ice margin itself. At such sites, data from six of which are shown on Fig. 11, sea-level is observed to first fall and then rise subsequent to ice sheet disintegration. On each part of this figure predictions are shown for two models which differ only in their lower mantle viscosities. The uniform viscosity model, whose predictions are shown by the squares, clearly predicts this observed non-monotonicity of the RSL signature at edge sites quite accurately. For the model whose lower mantle viscosity is increased even by a factor of 3, however, this non-monotonicity of the RSL prediction is completely removed (the predicted curves are denoted by the crosses). In the context of the Maxwell parameterization of the visco-

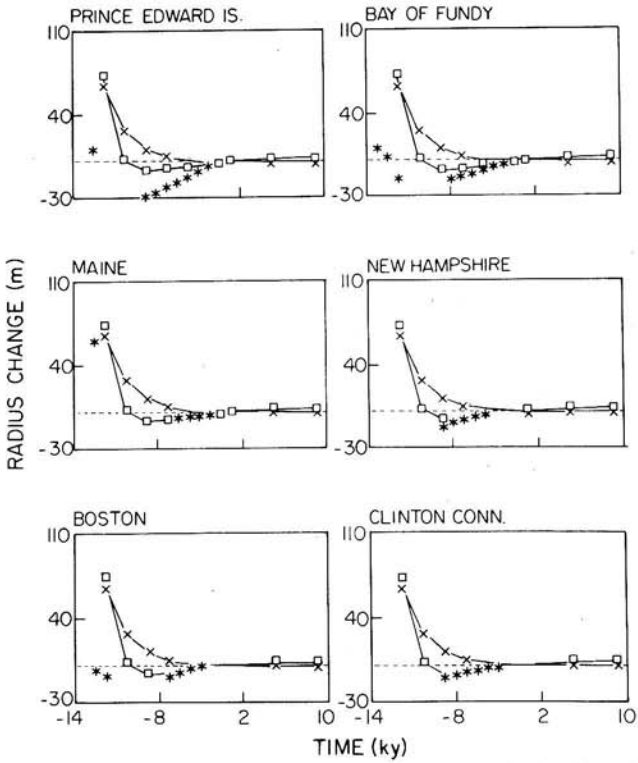

Figure 11. Comparisons between predicted and observed RSL data at six sites located near the margin of the Laurentian ice sheet. Predictions are shown for two models which differ from one another only in their lower mantle viscosities: the symbols (□) are for the uniform viscosity Maxwell model, whereas the symbols (x) denote the predictions of the model whose lower mantle viscosity is 3×10^{21} Pa s which should be compared to the upper mantle value of 10^{21} Pa s.

elasticity this is then a further observation which points strongly to a preference for uniform viscosity stratification.

The way in which elevated lower mantle viscosity affects the RSL predictions at such edge sites is by strongly inhibiting the propagation of the glacial forebulge during the isostatic adjustment process (Peltier 1974). This is illustrated by the depiction of the collapse on Figs 12 and 13 which shows the form of the surface deflection beyond the ice margin from sites in New Hampshire (NH), Maine (MN), and Brigantine (BR) in the north to Florida (FL) in the south as a function of time from 9000 to 1000 yr ago in 2 kyr intervals. Inspection of these data shows very clearly that increasing the viscosity of the lower mantle by even a factor of 3 very substantially reduces the region of non-monotonicity, while a factor of 10 increase eliminates it entirely. Also evident by inspection of these figures is the fact that the observed variation of RSL at sites on the southern flank of the forebulge should also be highly diagnostic of the contrast in viscosity between the upper and lower mantle. That this is in fact the case has been clearly shown in the recent extensive reanalysis of east coast RSL data presented in Peltier (1986) based upon the gravitationally self-consistent model of post-glacial sea-level variations embodied in 'the sea-level equation' (e.g. Clark *et al.* 1978; Peltier *et al.* 1978). This analysis has demonstrated that a slight increase of lower mantle viscosity seems to be *required* to fit the observations at the Florida

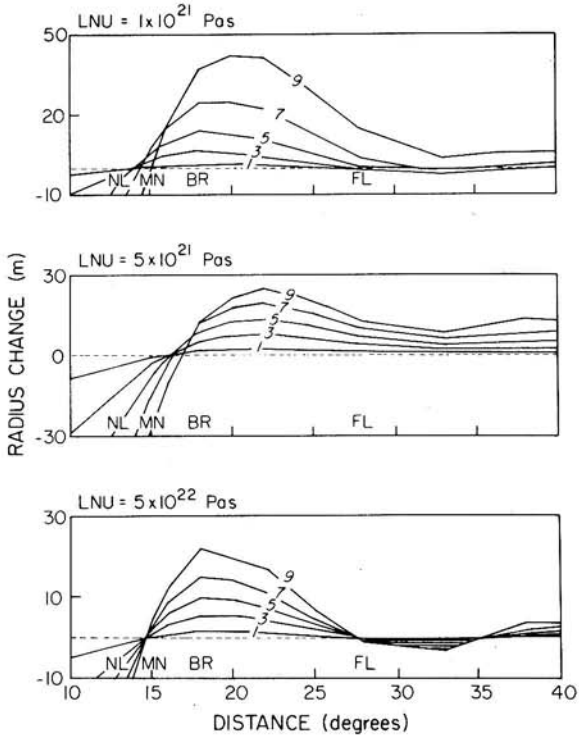

Figure 12. Constant time horizons, with ages labelled in thousands of years, illustrating the nature of forebulge collapse as a function of position for sites outside the ice margin. Each frame is for a Maxwell model with different lower mantle viscosity, the value of which is denoted by the label LNU at the top of each frame. The sites denoted NL, MN, BR and FL respectively denote the locations of the New Hampshire, Maine, Brigantine, and Florida sites at which ^{14}C data are available.

site since the uniform model predicts present-day occurrence of emergence of the land relative to the sea, whereas submergence is characteristic of the ^{14}C controlled RSL data. The contrast which is required to remove this misfit is very small, however, and an increase which is less than x2 is adequate to bring the predictions into accord with the data. Such an increase is not sufficient to prevent forebulge migration so that the RSL data at sites near the ice margin remain well fitted by model predictions. We will proceed to discuss below the compatibility of this almost uniform viscosity Maxwell model with other post-glacial rebound data.

3.2 FREE AIR GRAVITY ANOMALY AND $\dot{g}$ AS ADDITIONAL CONSTRAINTS ON THE RADIAL STRUCTURE OF THE MAXWELL MODEL

As mentioned in the introduction to this paper, the free air gravity anomalies observed over present-day centres of post-glacial rebound have been the cause of considerable controversy in the continuing debate concerning mantle viscosity. Jeffreys (e.g. 1972) for example often pointed to the apparent inability of the constant viscosity models of Haskell (1935, 1936) to fit both RSL and free air gravity data as evidence of the invalidity of the Newtonian viscous model of the rheology upon which Haskell's calculations were based. Walcott (e.g. 1970) has more recently suggested that the free air gravity data required that the lower

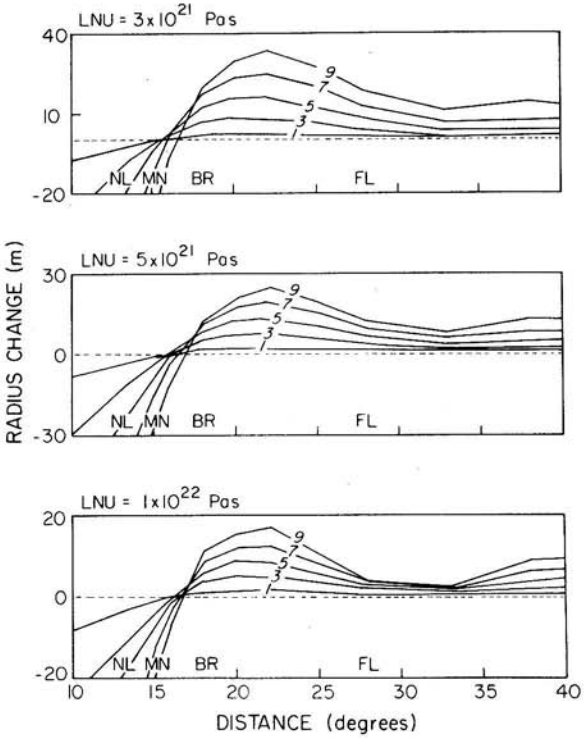

Figure 13. Same as Fig. 12 but for three different values of the lower mantle viscosity.

mantle viscosity be high. One way out of this dilemma recently suggested in Peltier & Wu (1982), Peltier (1982), Wu & Peltier (1983) and Peltier (1985a) is to postulate that some part of the internal mantle density stratification is able to induce a buoyant restoring force when the individual density horizons within it are deflected by the gravitational interaction of the planet with surface ice sheet loads. Peltier (1976) showed that if the seismic discontinuity at 670 km depth in the Earth was assumed to act as a non-adiabatic horizon in so far as glacial isostasy was concerned then the model supported a new mode of relaxation, which he labelled M1, which was efficiently excited by a surface load of sufficient spatial scale and which carried in excess of 10 per cent of the total relaxation at long wavelengths. Peltier & Wu (1982) showed that this was exactly what was required in order for the uniform viscosity model which was preferred to fit post-glacial RSL data to fit observed free air anomalies also. Fig. 14 provides a much more complete demonstration of this fact than any which we have previously presented. In (a) and (b) of this figure we show predicted peak present-day free air gravity anomalies over Laurentia and Fennoscandia respectively, for a series of different earth models which differ with respect to the amount of internal buoyancy provided by their mantle density stratifications. The models include the homogeneous layered models with properties listed in Table 1 and the seismically realistic model 1066B. Inspection of this figure demonstrates that as the amount of internal mantle buoyancy increases the models are able to fit the observed peak free air anomalies, denoted by the stippled regions, for smaller and smaller contrasts of viscosity between the upper and lower mantles. The models with the greatest internal buoyancy are able to fit the observed gravity anomalies for viscosity contrasts of the order of those required (and allowed) by the

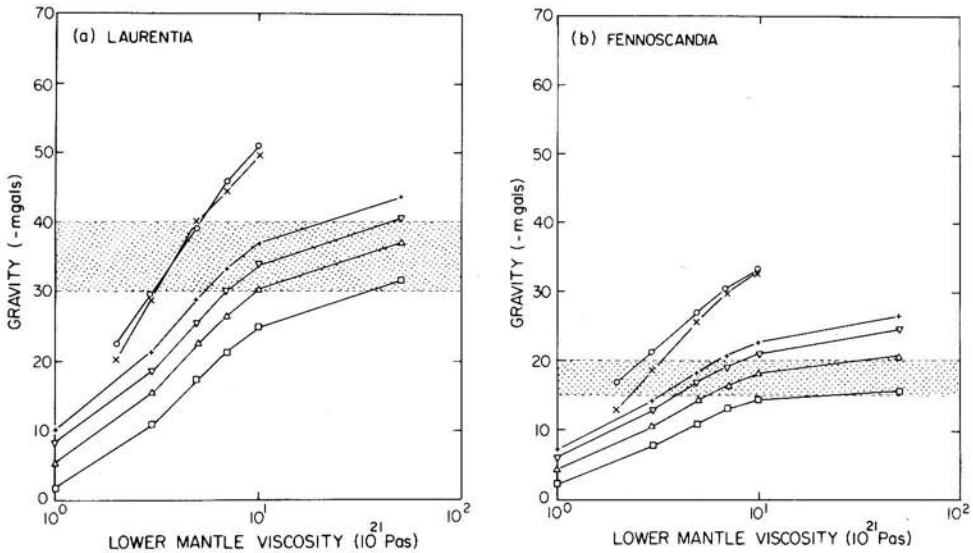

Figure 14. Comparisons of predicted and observed peak free air gravity anomalies for the Laurentian and Fennoscandian regions as a function of lower mantle viscosity in the Maxwell parameterization. Computations are shown at each site for a set of five different earth models which differ from one another only with respect to the amount of buoyancy which is contained in their mantles. These are respectively: □, for the model with no internal mantle buoyancy; Δ, for the model with a single 6.2 per cent increase at 670 km depth; Δ, for the model with a single 6.2 per cent increase at 670 km depth; ∇, for the model with 6.2 and 3.8 per cent increases at 670 and 420 km depth respectively; + for the model with a 12.4 per cent increase at 670 km depth; x, for 1066 B; 0, for PREM.

RSL data discussed previously. Also clear by inspection of these figures is the fact that for models without internal buoyancy the predicted free air anomalies are only marginally compatible with the observations even with an increase of viscosity by a factor of 10^2 from the upper mantle value of 10^{21} Pa s to the lower mantle. Such an increase is of course completely ruled out in the context of the Maxwell parameterization of the radial visco-elastic structure by RSL observations.

For the sake of completeness in the present discussion of the gravitational signature of the glacial isostatic adjustment process, we illustrate in Fig. 15 the dependence of the predicted free air anomaly as a function of lower mantle viscosity for a sequence of models based upon the same elastic structure (that in Table 1 which has an increase of density of 12.4 per cent across 670 km depth) but which have different upper mantle viscosities varying from 10^{20} to 10^{22} Pa s. Inspection of this figure shows that if the upper mantle viscosity were much less than 0.3×10^{21} Pa s then it would be rather difficult to fit the free air anomaly at all with this level of internal buoyancy no matter what the lower mantle viscosity might be. On the other hand for upper mantle viscosities even an order of magnitude higher than 10^{21} Pa s one does not substantially lower the required lower mantle values. Models with upper mantle viscosities too much in excess of 10^{21} Pa s are, however, completely ruled out by the RSL data.

One additional datum which we have not considered at all in our previous analyses of glacial isostatic adjustment effects concerns the time variation of g over the centres of rebound. Although there do not currently exist observations of $\dot{g}$, the new absolute g instruments which have become available recently (Zumberge, Rinkler & Faller 1982; Zumberge, Faller & Gschwind 1983) will eventually make such measurements entirely

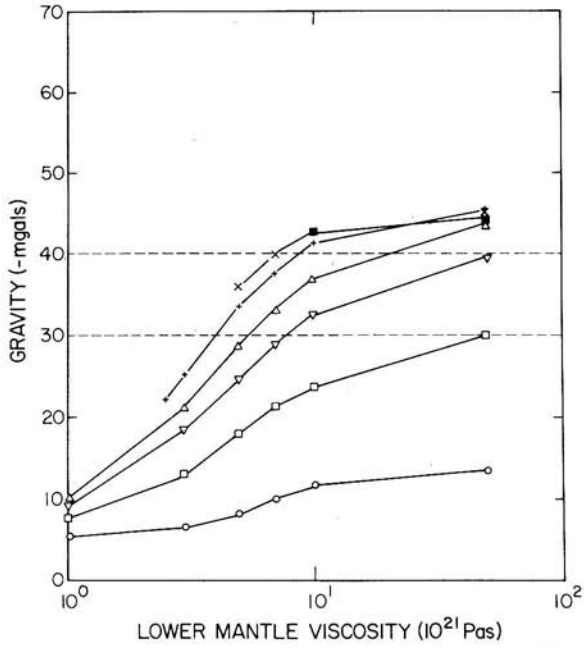

Figure 15. Peak free air gravity anomaly over Hudson Bay as a function of lower mantle viscosity for Maxwell models which differ only in the value of the viscosity in the upper mantle. The elastic basic state employed in the calculations is the one with a single 12.4 per cent density jump at 670 km depth in the mantle. The upper mantle viscosity values are respectively: 10^{20} Pa s (0), 0.3×10^{21} Pa s (□), 0.6×10^{21} Pa s (▽), 10^{21} Pa s (△), 2.5×10^{21} Pa s (+), 10^{22} Pa s (■).

feasible, if not routine. As we will demonstrate here, such measurements may be particularly useful as an additional means of distinguishing between different models of the radial visco-elastic stratification. Fig. 16 shows predicted present-day $\dot{g}$ at the centre of the model Laurentian (a) and Fennoscandian (b) disc loads as a function of lower mantle viscosity with the upper mantle value held fixed to 10^{21} Pa s. Again predictions are shown both for the set of multiple homogeneous layer models with properties listed in Table 1 and for 1066B and PREM. Inspection shows that this datum is also a very strong discriminant between models which have internal buoyancy and models which do not. The difference in the predicted $\dot{g}$ signal between the 'seismically realistic' and multiple homogeneous layered models is about 50 per cent and is only moderately dependent upon the upper mantle–lower mantle viscosity contrast. Since the question of how much internal buoyancy the mantle may contain is a rather important one from a geodynamic perspective, every effort should be made to collect all of the observational evidence which might be brought to bear on it. We have shown here that $\dot{g}$ is such a datum and strongly suggest that the new absolute g instruments should be deployed in Canada and Fennoscandia to attempt the measurement.

3.3 $\dot{J}_2$ AS A CONSTRAINT ON THE RADIAL STRUCTURE OF THE MAXWELL MODEL

As recently pointed out in Peltier (1983, 1985b) the new observation of $\dot{J}_2$ with the *LAGEOS* satellite, and therefore of the non-tidal acceleration of rotation which is related to it, provides a particularly important additional constraint on the contrast in viscosity between the upper and lower mantle. The special importance of this observation is for two reasons.

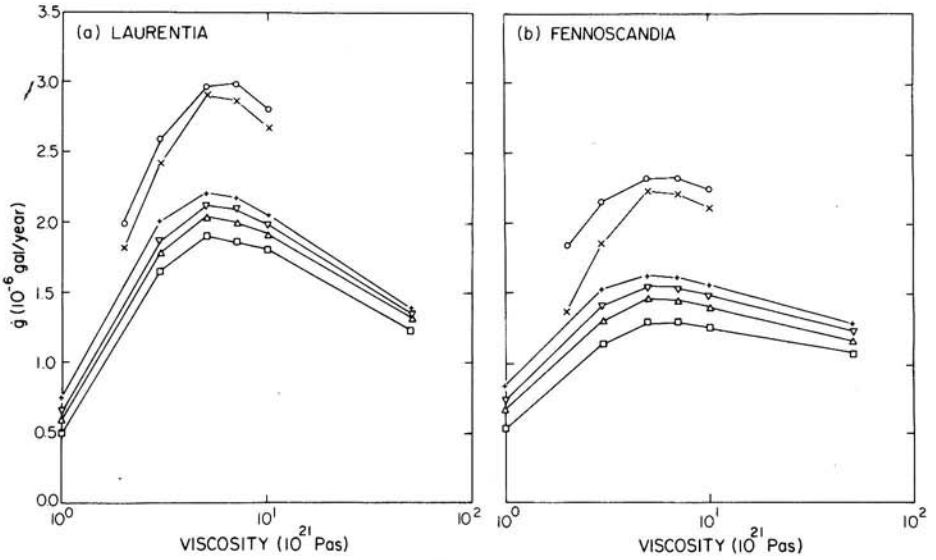

Figure 16. $\dot{g}$ predictions for the centres of both the Laurentian (a) and Fennoscandian (b) loads. The predicted peak $\dot{g}$ is shown as a function of lower mantle viscosity in the Maxwell parameterization for the same set of models described in the caption to Fig. 14. These models differ from one another only with respect to the amount of buoyancy in their mantles.

First, because of the physical effect observed, the acceleration of the node of the satellite orbit is most, if not quite exclusively (Alexander 1983), sensitive to the degree two harmonic of the deformation spectrum; the datum samples the planet to great depth and therefore should see the contrast between upper and lower mantle particularly clearly. Secondly, and of particular importance, is the fact that this datum, unlike the free air gravity anomaly, is not particularly sensitive to the presence or absence of internal mantle buoyancy nor is it sensitive to the thickness of the lithosphere (Peltier 1985b). It is therefore the datum best suited to provide an unambiguous measure of the required viscosity ratio.

Fig. 17 shows predictions of $\dot{J}_2$ for a sequence of homogenous layered earth models with density contrasts of 3.8 and 6.2 per cent respectively across the 420 and 670 km depth horizons, with lithospheric thickness fixed at 120 km and upper mantle viscosity to 10^{21} Pa s in (a). Fig. 17(a) illustrates the influence on the predicted non-tidal acceleration and $\dot{J}_2$ of the number of ice sheets employed in the theoretical calculation. The curve marked with the crosses shows the variation of the prediction when only a single sheet (the Laurentian) is employed to force the rotational response. The curve marked with the plus symbols is for forcing which consists of the sum of the Laurentian and Fennoscandian ice sheets, while the final curve marked with the squares shows the result obtained when all three ice sheets (now including the West Antarctic ice sheet) are employed in the calculation. As discussed at length in Peltier (1982, 1983) there are two possible values of the lower mantle viscosity which are equally acceptable in the context of the Maxwell parameterization of the radial viscoelastic structure, one near 10^{21} Pa s and another near 10^{23} Pa s. On this plate the short dashed line denotes the region within which the observation of Yoder *et al.* (1983) lies ($[-7.0 \pm 0.6] \times 10^{-11}\,\mathrm{yr}^{-1}$) whereas the long dashed lines denote the independent result of Rubincam (1984) ($[-5.2 \pm 1.1] \times 10^{-11}\,\mathrm{yr}^{-1}$). Clearly if the former observation is more nearly correct the two allowed values of lower mantle viscosity (or

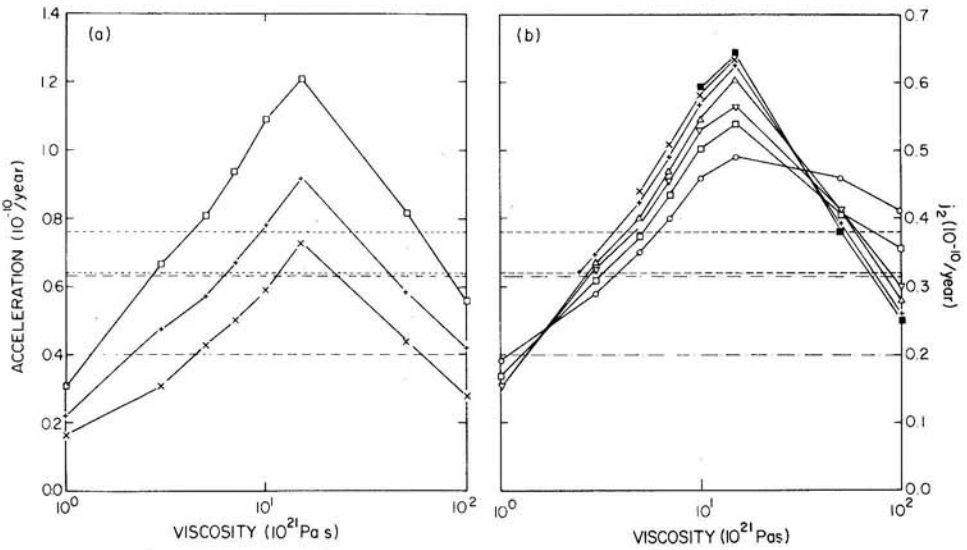

Figure 17. Predicted and observed $\dot{J}_2$ and non-tidal acceleration of rotation as a function of lower mantle viscosity in the Maxwell model. The elastic basic state is the one with 3.8 and 6.2 per cent increases of density at 420 and 670 km depth respectively, the lithospheric thickness is 120.7 km and the upper mantle viscosity for the calculations in plate (a) is fixed at 10^{21} Pa s. (a) Results are shown for a model containing forcing from only the Laurentian ice sheet (x), for one including both the Laurentian and Fennoscandian ice sheets (+), and for one including Laurentian, Fennoscandian, and Antarctic forcing (□). (b) Results are shown for the three ice sheet model as a function of lower mantle viscosity in the Maxwell parameterization. The different individual predictions are for models which differ only in their upper mantle viscosities. The values of these viscosities are the same as for the corresponding symbols in the caption to Fig. 15.

ranges of allowed values of lower mantle viscosity) are more closely spaced ($\sim 4 \times 10^{21}$ and $\sim 7 \times 10^{22}$ Pa s) than they are if the latter observation is to be preferred ($\sim 2 \times 10^{21}$ and $\sim 10^{23}$ Pa s). In either case, however, the upper of the two roots is completely ruled out by the RSL observations discussed previously. The lower root is the only acceptable solution and accords very well with the stratification of viscosity required by both the sea-level and free air gravity observations.

Fig. 17(b) extends the results described above by illustrating the variation of this double root structure for models with a variable upper mantle viscosity. These analyses are all based upon the same elastic structure as was employed in the construction of (a) and all calculations employed a forcing function which includes all three ice sheets and the saw-tooth approximation to glaciation history shown in Fig. 2. The lithospheric thickness is again fixed at 120 km and the different curves on this plate are for models with upper mantle viscosities varying from 10^{20} to 10^{22} Pa s. Inspection of this figure shows that although the upper root for lower mantle viscosity rapidly increases as the upper mantle viscosity is reduced, the lower root remains relatively stable. Since this is the only physically admissible solution in the context of the Maxwell parameterization of the viscoelasticity, the lower mantle viscosity is rather tightly constrained by the $\dot{J}_2$ datum. Although we could continue in this section to review the additional constraint on the Maxwell model which are delivered by the polar wander observed in the ILS path, this analysis has been discussed at length in the recent papers by Wu & Peltier (1984) and Peltier (1984) and we have nothing further to add which would be useful here. In the following section, however, which

describes the fits to the rebound observations which have been obtained with the alternate Burger's body representation of the viscoelasticity, this datum will be shown to play an especially interesting and useful role.

4 Results based upon the Burger's body parameterization

The above analyses should suffice to demonstrate anew the fact mentioned in the introduction, that when a Maxwell parameterization of the internal viscoelastic structure is employed to represent the viscoelasticity then one is led to conclude that the viscosity of the mantle must be rather uniform. As we also mentioned in the introduction this may pose something of a dilemma because several lines of evidence have recently converged which suggest that the steady state shear viscosity of the lower mantle may be much higher than the steady state shear viscosity of the upper mantle. The models preferred by Richards & Hager (1984) in fact have a preferred contrast of two orders of magnitude with the upper mantle having the same viscosity near 10^{21} Pa s delivered by the glacial rebound analyses and the lower mantle a viscosity of 10^{23} Pa s. As we also stated in the introduction, although it may be somewhat premature to accept this analysis at face value it is nevertheless interesting to ask the question as to what this analysis would imply if its validity were to withstand the tests to which it is currently being subject. The immediate implication of this result is that the lower mantle viscosity which post-glacial rebound is sensing must be a transient component of the viscosity spectrum as suggested by Weertman (1978) rather than the steady state component. In Section 2 of this paper we showed in terms of the 3-D Burger's body analogue of Peltier *et al.* (1981) that a transient component of the viscosity spectrum could masquerade as a steady state component under certain conditions in which the elastic defect associated with the transient relaxation was very large (i.e. $\mu_2 \ll \mu_1$ in terms of the parameters of this analogue). In the present section of this paper we will address the question of how large this elastic defect must be in order to allow the Burger's body to deliver fits to the rebound data which are as acceptable as those obtained through the use of the Maxwell analogue. As we will proceed to show, it is only in the limit $\mu_2 \ll \mu_1$, in which case the Burger's body degenerates to a Maxwell solid governed by the effective viscosity $\nu_{\text{eff}} = \nu_1 \nu_2/(\nu_1 + \nu_2)$, that acceptable fits to the data may be obtained. This is rather convenient since it implies that previous inferences of effective lower mantle viscosity obtained with the Maxwell analogue may be simply interpreted as transient rather than steady state values if we should be required to do so as new information becomes available concerning the implications of the isostatic geoid height anomalies analysed by Richards & Hager (1984).

In producing the tests of the Burger's body rheology discussed below, we will assume that the Richards & Hager (1984) analysis is correct and therefore that the steady state shear viscosity ν_1 of the Burger's body equals 10^{21} Pa s in the upper mantle and 10^{23} Pa s in the lower mantle. With the parameters of the instantaneous elastic structure λ_1, μ_1 and ρ fixed to one of the profiles employed previously we will then seek to determine the lower mantle values of ν_2 and μ_2 which enable the Burger's body model to fit the observations. The value of ν_2 in the upper mantle and lithosphere will be assumed infinite so that in this region of the Earth the rheology is identical to that employed previously. Since all of the different signatures of the glacial isostatic adjustment process are dependent upon the relaxation time and amplitude spectra illustrated for Maxwell models in Figs 3–8, the first step in testing the applicability of the new Burger's body representation is to determine these spectra for the new rheological structures. One example will suffice to illustrate the rather substantial increase in complexity of these spectra which is produced even when the

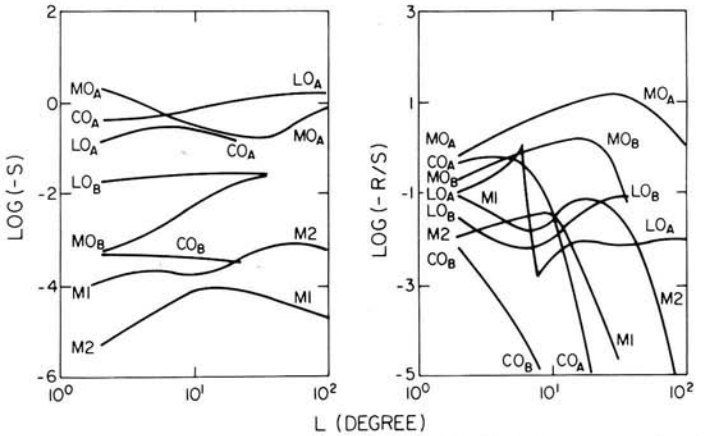

Figure 18. Relaxation time and amplitude spectra for the Burgher's body model with $\mu_2/\mu_1 = 0.01$, $\nu_2 = 10^{21}$ Pa s in the lower mantle and $\nu_2 = \infty$ elsewhere, $\nu_1 = 10^{21}$ Pa s in the upper mantle and $\nu_1 = 10^{23}$ Pa s in the lower mantle in accord with the results of Richards & Hager (1984). The elastic basic state employed to do the computation of these spectra is that for the model with density jumps of 3.8 and 6.2 per cent at 420 and 670 km depths respectively. Comparing these spectra with those shown in Fig. 6 for the corresponding Maxwell model demonstrates that the main difference is the introduction of the two new modal branches denoted MOB and COB due to the multiplicity of viscosities required to describe the radial structure of the simple Burgher's body transient model.

transient is restricted to the lower mantle as discussed above. Fig. 18 shows spectra for a model with $\mu_2/\mu_1 = 0.01$ and $\nu_2 = 10^{21}$ Pa s in the lower mantle. Inspection demonstrates that the introduction of the transient component of rheology in this restricted region introduces three new modal branches into the relaxation diagram which are labelled MOB, COB, and LOB, which are respectively new mantle, core, and lithosphere modes, which are supported by the new transient viscosity ν_2 which is required to represent the structure. This figure should be compared with Fig. 6, which is for a model with identical elastic structure but based upon the Maxwell analogue. In order to understand the way in which this greatly increased spectral complexity modifies the values required for the parameters which describe the structure, we must proceed to re-compute each of the different signatures of the rebound process discussed in the last section. The results of these computations are described in the following subsections.

4.1 RSL CONSTRAINTS ON THE RADIAL STRUCTURE OF THE BURGER'S BODY MODEL

Fig. 19 demonstrates the nature of the fits to the RSL data for a Burger's body model which has $\mu_2/\mu_1 = 0.1$ in the lower mantle, for three calculations which differ from one another only in the choice of the magnitude of the transient viscosity ν_2 which governs the lower mantle relaxation. Results are shown for six sites which are located at various distances from the centre of the model Laurentian disc load. All calculations employed the homogeneous layered approximation to the radial elastic structure which has density discontinuities of 3.8 and 6.2 per cent at 420 and 670 km depth respectively. At each model site three calculations are shown for $\nu_2 = 10^{21}$, 10^{22} and 10^{23} Pa s. Since it will be our contention in consequence of the results obtained for other signatures of the isostatic adjustment process, that even the relatively small value of $\mu_2/\mu_1 = 0.1$ employed here is too

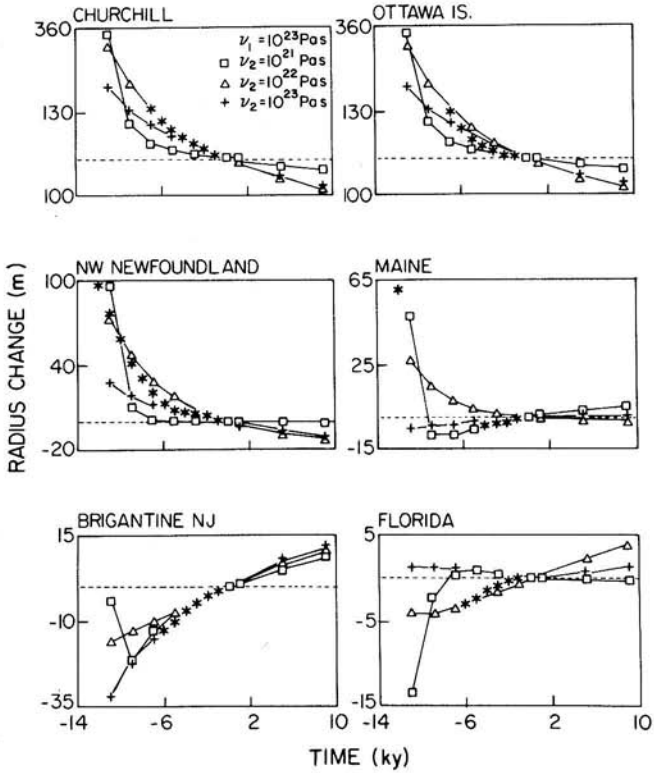

Figure 19. Comparison of observed and predicted RSL data at six North American sites for the Burger's body rheology with $\mu_2/\mu_1 = 0.1$. The elastic basic state is the same as was employed in the computation of the spectra for $\mu_2/\mu_1 = 0.01$ shown in Fig. 18. The lithospheric thickness of the Burger's body is fixed at 120.7 km, $\nu_1 = 10^{21}$ Pa s and $\nu_2 = \infty$ in the upper mantle, and $\nu_1 = 10^{23}$ Pa s in the lower mantle. The different RSL predictions on each part are for models with lower mantle ν_2 values of: 10^{21} Pa s (□), 10^{22} Pa s (Δ), and 10^{23} Pa s (+).

large to accommodate the rebound observations, it is important to grasp clearly the implications of the fits to the RSL data in Fig. 19.

At the Churchill, Ottawa Islands and NW Newfoundland sites the choice $\nu_2 = 10^{21}$ Pa s does not provide an adequate fit to the observations. At such sites the relaxation predicted by the transient model with $\nu_2 = 10^{21}$ Pa s displays extremely rapid initial relaxation and consequently predicts far too slow a present-day rate of emergence and too little relaxation in the last 6 kyr to fit the data. Increasing ν_2 alleviates this problem but the increase to $\nu_2 = 10^{22}$ Pa s is too great. At Churchill the preferred ν_2 is near 5×10^{21} Pa s while at the Ottawa Islands and NW Newfoundland sites the preferred ν_2 is closer to 2×10^{21} Pa s. At edge sites, represented by Maine in the collection shown on Fig. 20, increasing ν_2 by even a factor of 5 completely eliminates the non-monotonic signature from the uplift prediction which is required to fit the observations. At this site a value of ν_2 of 2×10^{21} Pa s would be marginally acceptable. The Brigantine NJ site is on the crest of the glacial forebulge and as such is more sensitive to lithospheric thickness than to lower mantle viscosity. In fact the model with highest ν_2 fits these data best but the sensitivity to variations of the parameter is so small that any of the three values is equally acceptable. This comparison demonstrates that with the relatively high value of $\mu_2/\mu_1 = 0.1$, US east coast RSL data can be fitted with

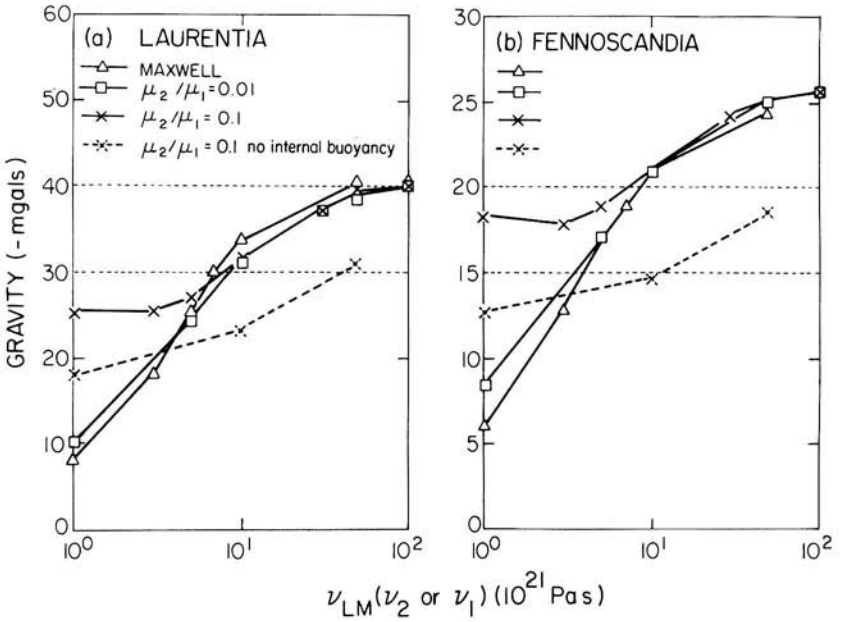

Figure 20. Predicted peak free air gravity anomalies at the centres of Laurentia (a) and Fennoscandia (b) as a function of lower mantle viscosity in the Burger's bodies with $\mu_2/\mu_1 = (0.1, 0.01)$ in which cases the lower mantle viscosity varied is the transient value ν_2, and in the Maxwell analogue to which the Burger's body converges in the limit $\mu_2 \to 0$ in which case the lower mantle viscosity varied is the steady state value ν_1. The elastic basic state employed in these calculations is the one in which there are density increases of 3.8 and 6.2 per cent at 420 and 670 km depth respectively. Also shown on these separate plates by the dashed lines are the predicted free air gravity anomalies for the Burger's body analogue with $\mu_2/\mu_1 = 0.1$ using an elastic basic state in which the mantle contains no internal buoyancy. Clearly, even in the Burger's body case considerable internal buoyancy appears to be required to fit the observed free air anomalies but perhaps somewhat less than for the Maxwell model.

a thinner lithosphere than has been shown to be required with the Maxwell parameterization according to the discussion of Peltier (1984). At the Florida site, neither the model with very weak or very strong stratification of viscosity is acceptable. As pointed out in Peltier (1986) some small increase in lower mantle viscosity is required to remove the raised beaches predicted at this site by the homogeneous model when the Maxwell parameterization is employed. The same is clearly true with the Burger's body parameterization. Although this characteristic misfit of the homogeneous model is clearly eliminated by the increase of ν_2 to the value of 10^{22} Pa s, an increase to the lower value of $2-3 \times 10^{21}$ Pa s is similarly effective. The basic conclusion from these analyses is therefore that from the point of view of the RSL data the Burger's body rheology with $\mu_2/\mu_1 = 0.1$ and $\nu_2 = 2 \times 10^{21}$ Pa s in the lower mantle will provide acceptable agreement. Values of ν_2 higher than this are ruled out by the observed non-monotonicity of the sea-level record at sites near the ice margin just as similarly high values of the steady state viscosity ν_1 were ruled out in the context of the Maxwell parameterization. In the Burger's body model with $\mu_2/\mu_1 = 0.1$ the parameter ν_2 is therefore playing the same role as that played by ν_1 in the Maxwell analyses. The asymptotic analysis of the Burger's body in the limit $\mu_2 \to 0$ shows that this should be the case. The sea-level analyses discussed here suggest that $\mu_2/\mu_1 = 0.1$ is sufficiently close to zero that the asymptotic result already obtains. In the following subsections we will address

the question as to whether the other signatures of the adjustment process agree that this particular representation of the transient is equally acceptable to them.

4.2 FREE AIR GRAVITY ANOMALIES AS AN ADDITIONAL CONSTRAINT ON THE RADIAL STRUCTURE OF THE BURGER'S BODY MODEL

Fig. 20 provides a parallel analysis to that in Fig. 14 for the peak free air gravity anomalies at the centres of the Laurentian and Fennoscandian loads. On each plate the predicted peak free air anomaly is shown as a function of lower mantle viscosity (either ν_2 with $\nu_1 = 10^{23}$ Pa s for the Burger's body analogues, or ν_1 for the Maxwell analogue). For the Burger's body representations, calculations are shown for $\mu_2/\mu_1 = (0.1, 0.01)$ in the lower mantle and these results are compared on each plate with those for the same Maxwell model with 6.2 and 3.8 per cent density discontinuities in the elastic structure as is being employed for all calculations in this subsection. Since we have previously demonstrated that free air gravity anomalies are extremely sensitive to the presence of internal buoyancy in the mantle, we have also shown on each plate (dashed lines) the variation of the predicted free air gravity anomaly as a function of ν_2 for the Burger's body with $\mu_2/\mu_1 = 0.1$ with no internal buoyancy.

Inspection of the data shown on this figure demonstrates that for sufficiently large lower mantle $\nu_2 \gtrsim 6 \times 10^{21}$ Pa s (or ν_1 in the Maxwell analogue) the predictions of all three models with internal buoyancy are essentially identical. In the region of small viscosity contrast with $\nu_2 \lesssim 6 \times 10^{21}$ Pa s, however, the prediction of the model with $\mu_2/\mu_1 = 0.1$ differs substantially from that of either the model with $\mu_2/\mu_1 = 0.01$ or the Maxwell model. In terms of

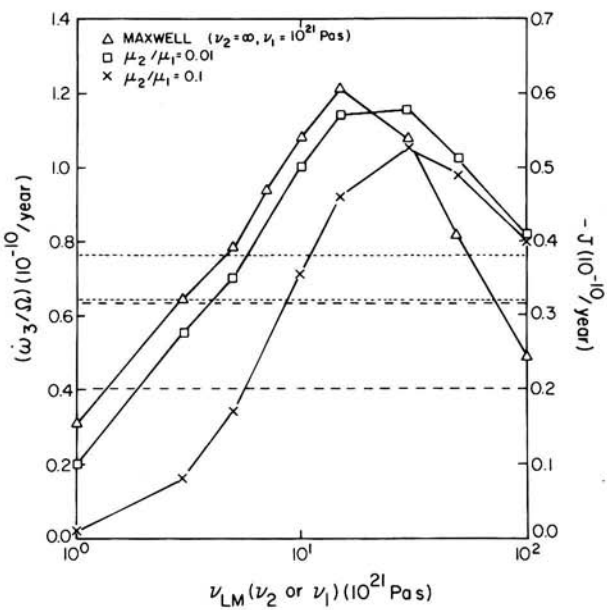

Figure 21. Predicted $\dot{J}_2$ and the associated nontidal acceleration of rotation as a function of lower mantle viscosity for both the Burger's body rheologies with $\mu_2/\mu_1 = (0.1, 0.01)$ and for the Maxwell analogue to which the Burger's body degenerates in the limit $\mu_2 \to 0$. The upper and lower horizontal dashed lines on this plate correspond respectively to the observed values based upon the analyses of *LAGEOS* data by Yoder *et al.* (1983) and Rubincam (1984).

the free air gravity anomaly it is therefore clear that $\mu_2/\mu_1 = 0.1$ is not sufficiently small for the asymptotic condition to obtain because it is the hallmark of this condition that the transient model will behave exactly as its Maxwell counterpart. With $\mu_2/\mu_1 = 0.01$ this asymptotic condition obtains to quite a high degree of approximation for all ν_2. With $\mu_2/\mu_1 = 0.1$, however, the free air anomalies predicted by the transient model with weak viscosity contrast are higher than those of the model with $\mu_2/\mu_1 = 0.01$ or of the corresponding Maxwell model. This increase is sufficient, in the case of the smaller Fenno-scandian ice cap, to allow the strong transient model to fit the free air anomaly without any increase of viscosity at all. In the case of the Laurentian region, however, some increase of viscosity is still required to fit the observation, although somewhat less than would be required in the weak transient ($\mu_2/\mu_1 = 0.01$) or equivalent Maxwell case. The dashed lines on this figure, which are the predictions for strong transient models ($\mu_2/\mu_1 = 0.1$) with no internal buoyancy demonstrate that even in this case, in which the transience contributes efficiently to maintaining the anomaly, considerable internal buoyancy does seem to be required to fit the data as has been found to be the case for the Maxwell model (see Section 3.2).

On the basis of the calculations described here models with modest viscosity contrast in either the transient Burger's body or Maxwell formulations are required by both the RSL and free air gravity observations. Furthermore there is no strong preference for the weak transient ($\mu_2/\mu_1 = 0.01$) as compared to the strong transient ($\mu_2/\mu_1 = 0.1$) in so far as these data are concerned. We will see that this is not the case in so far as rotation effects are concerned and we turn next to a discussion of them.

4.3 $\dot{J}_2$ AS A CONSTRAINT ON THE RADIAL STRUCTURE OF THE BURGER'S BODY MODEL

The same sequence of models employed to perform the free air gravity anomaly computations shown on Fig. 20 has been used to make the present-day $\dot{J}_2$ predictions shown on Fig. 21. In this diagram we show the model prediction as a function of lower mantle viscosity ν_2 for the Burger's bodies with $\mu_2/\mu_1 = (0.1, 0.01)$, and as a function of lower mantle viscosity ν_1 for the Maxwell model. Again the two sets of horizontal dashed lines represent the region within which the separate $\dot{J}_2$ observations of Yoder *et al.* (1983) and Rubincam (1984) are found. As mentioned previously and discussed at length in Peltier (1985b) the $\dot{J}_2$ observation is particularly important as it is relatively insensitive to either lithospheric thickness or to internal buoyancy. This makes the results illustrated especially important from the point of view of the issue as to what values of μ_2/μ_1 are allowed (required) by the rebound observations. Inspection of this figure shows that with $\mu_2/\mu_1 = 0.1$ the viscosity contrast between the upper and lower mantle must be about one order of magnitude in order to reconcile the value of $\dot{J}_2$ inferred from the *LAGEOS* satellite tracking data. As mentioned previously this high contrast is not acceptable from the point of view of the RSL record. In order to fit the *LAGEOS* observation with models having sufficiently low contrast as to be acceptable from these other points of view requires that the ratio μ_2/μ_1 be reduced substantially below the value of 0.1. A value of $\mu_2/\mu_1 = 0.01$, for which calculations are also shown in this figure, reduces the required contrast near to the same factor of 3 as was delivered by the Maxwell parameterization for which calculations are also shown on Fig. 21 for comparison purposes. With this very small value of the relaxed modulus the Burger's body has become very close to the asymptotic $\mu_2 = 0$ conditon for which the solid behaves as a Maxwell solid with effective viscosity $\nu_{\text{eff}} = \nu_1\nu_2/(\nu_1 + \nu_2)$ as far as the $\dot{J}_2$ observation is concerned. The necessity of having such a small value of μ_2/μ_1

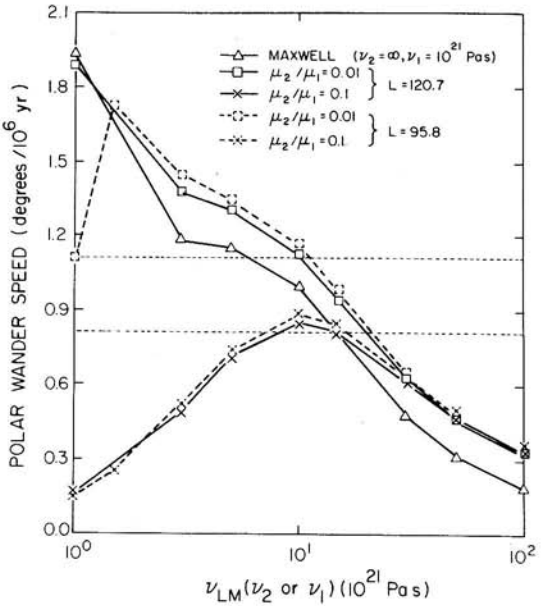

Figure 22. Predicted polar wander speed as a function of lower mantle viscosity for the Burger's body rheologies with $\mu_2/\mu_1 = (0.1, 0.01)$ in which case the lower mantle viscosity varied is the transient value ν_2, and for the Maxwell model to what the Burger's body degenerates in the limit $\mu_2 \to 0$ in which case the lower mantle viscosity varied is the steady state value ν_1. The solid curves on this figure are predictions for models with lithospheric thickness 120.7 km while the dashed curves are the predictions of models with lithospheric thickness of 95.8 km.

in the context of the Burger's body parameterization is further reinforced by the polar wander datum which is discussed below.

4.4 POLAR WANDER SPEED AS A FURTHER CONSTRAINT ON THE RADIAL STRUCTURE OF THE BURGER'S BODY MODEL

As mentioned in the introductory section of this paper, analysis of the ILS (International Latitude Service) record of the polar motion has established (e.g. Vincenti & Yumi 1969, 1970) that there is a secular drift of the pole currently taking place at the rate of (0.95 ± 0.15) degree/10^6 yr towards eastern Canada. Although Munk & Revelle (1952) believed that this observation required some current variation of surface load to be occurring, and suggested that this might be due to the melting of ice on Greenland and/or Antarctica, recent theoretical analyses have established that such present-day unsteadyness of the surface load is not required to understand this observation (Peltier 1982; Wu & Peltier 1984). These new analyses have in fact established that both the observed direction and speed of polar wander are exactly what is expected in response to forcing of polar motion by the 10^5 yr periodic glacial cycle which has dominated the last 700–800 kyr of Earth history according to $\delta^{18}0$ data. The nature of the theoretical solution for the forced polar wander given in equation (14) is such that the response is a strong function of all aspects of the radial viscoelastic structure including the lithospheric thickness as pointed out in Peltier & Wu (1983) and Wu & Peltier (1984), the internal buoyancy, and the contrast in viscosity between the upper and lower mantle.

Fig. 22 shows predictions of polar wander speed for a sequence of models which includes the same three basic types as were used in the previous discussion of the $\dot{J}_2$ datum. The predicted present-day speed is shown as a function of the lower mantle transient viscosity ν_2 (for the two Burger's bodies with $\mu_2/\mu_1 = 0.1$ and 0.01) and of the lower mantle steady state viscosity ν_1 (for the Maxwell analogue). All calculations employ the model with density discontinuities of 3.8 and 6.2 per cent at 420 and 670 km depth respectively. These three models have all been assumed to have lithospheric thicknesses of 120.7 km. Also shown on these figures are predictions for the two Burger's body models with their lithospheric thicknesses slightly reduced to 95.8 km (dashed lines). It is important to understand that the lithospheric thickness to which the polar motion datum is sensitive is presumably close to a planetary average thickness. Since the average thickness of oceanic lithosphere may be of the order of 60–70 km, even if the continental lithosphere is as thick in places as the 200 km which Peltier (1984, 1986) has suggested, the globally averaged thickness could be somewhat lower still than the slightly reduced value of 95.8 km which has been employed for these additional calculations.

Inspection of the computational results presented on Fig. 22 again demonstrates the fact that the predictions for the transient model with $\mu_2/\mu_1 = 0.01$ are very close to those for the Maxwell model, as expected on the basis of the asymptotic result expressed by equation (6) for the shear modulus $\mu(s)$ in the limit $\mu_2 \to 0$. With $\mu_2/\mu_1 = 0.1$, on the other hand the polar wander speed predicted in the case of weak viscosity stratification is reduced by more than an order of magnitude from that for the transient model with $\mu_2/\mu_1 = 0.01$ or for the Maxwell equivalent. Although the transient rheology with $\mu_2/\mu_1 = 0.01$ fits the data only in the case of large viscosity contrast ($\sim \times 10$ increase from the upper to the lower mantle) the model with $\mu_2/\mu_1 = 0.1$ barely comes within a standard error of the observation (i.e. within the horizontal dashed lines) and this is only for the same relatively high viscosity contrast. The influence of lithospheric thickness variations on these fits is however rather interesting as demonstrated by the dashed lines for each of the two transient models. Except for the region of low viscosity contrast ($\lesssim \times 2$) the slight reduction of lithospheric thickness generally causes a slight increase of the speed prediction. At very low contrasts the sense of the variation of speed is reversed and although the magnitude of the speed reduction for the $\mu_2/\mu_1 = 0.1$ model is small, that for the $\mu_2/\mu_1 = 0.01$ model is very large indeed, so large as to allow this model to fit the observation with no viscosity contrast at all. Further decreases of lithospheric thickness will clearly allow the $\mu_2/\mu_1 = 0.01$ model to fit the observation for the same modest contrasts of viscosity as are required by the sea-level and non-tidal acceleration of rotation data. On the other hand we could alternatively consider the lithospheric thickness fixed at 120.7 km and fit the datum with weak contrast by choosing $0.01 < \mu_2/\mu_1 < 0.1$. In any event a value of μ_2/μ_1 as large as 0.1 is as firmly rejected by the polar wander speed observation as it was by the $\dot{J}_2$ datum discussed in Section 4.3.

5 Conclusions

The main new idea which was developed in this paper concerns the possibility that the deep mantle viscosity inferred from the analysis of post-glacial rebound data using a Maxwell parameterization of the radial viscoelastic structure is interpretable, if necessary, as a transient value rather than that which governs steady state creep. This is possible because only transient models characterized by a very large elastic defect are plausible models for the understanding of the various signatures of the rebound process. When $\mu_2/\mu_1 \ll 1$ then the Burger's body representation of the combined effects of transient and steady state creep degenerates to a Maxwell analogue with an effective viscosity $\nu_{\text{eff}} = \nu_1\nu_2/(\nu_1 + \nu_2)$. In a

region in which the steady state viscosity ν_1 is large, such as the lower mantle according to the analyses of Richards & Hager (1984), $\nu_1 \gg \nu_2$ and $\nu_{\text{eff}} \simeq \nu_2$ which is the transient value. This may be a useful result if the analyses of Richards & Hager are reconfirmed by the application of more realistic models of the Earth to invert for the viscosity structure than those which these authors have employed.

One additional new idea which we introduced in the course of the preceding discussions is the notion that $\dot{g}$ observations may be feasible in the near future using new absolute g instruments (Zumberge *et al.* 1982, 1983). We have shown this datum to be rather sensitive to the existence of the internal byoyancy in the mantle which seems to be required to fit observed free air gravity anomalies over the main centres of post-glacial rebound. Whether or not such buoyancy actually exists is such an important point from a geodynamic perspective (Peltier 1985a) that a serious effort would appear warranted to deploy these new instruments in both eastern Canada and north-western Europe in order to develop the required data sets. In the same connection we have pointed out that it may be possible to some extent to trade-off the strength of the transient component of the relaxation in the lower mantle of the model against internal mantle buoyancy.

References

Alexander, J. C., 1983. Higher harmonic effects of the Earth's gravitational field from postglacial rebound as observed by *LAGEOS*, *Geophys. Res. Lett.*, **10**, 1085–1087.

Clark, J. A., Farrell, W. E. & Peltier, W. R., 1978. Global changes in postglacial sea level: a numerical calculation, *Quat. Res.*, 9, 265–287.

Courtney, R. C., 1982. On the rheology of the oceanic and continental lithospheres, *MSc thesis*, Dalhousie University.

Dicke, R. H., 1966. The secular acceleration of the earth's rotation and cosmology, in *The Earth Moon System*, eds Marsden, B. G. & Cameron, A. G. W., Plenum Press, New York.

Dziewonski, A. M., 1984. Mapping the lower mantle: determination of lateral heterogeneity of *P* velocity up to degree and order 6, *J. geophys. Res.*, **89**, 5929–5952.

Dziewonski, A. M. & Anderson, D. L., 1981. Preliminary reference earth model, *Phys. Earth planet. Int.*, **25**, 297–356.

Dziewonski, A. M., Hager, B. H. & O'Connell, R. J., 1977. Large scale heterogeneities in the lower mantle, *J. geophys. Res.*, **82**, 239–255.

Ellsworth, K., Schubert, G. & Sammis, C. G., 1985. Viscosity profile of the lower mantle, *J. geophys. Res.*, in press.

Farrell, W. E. & Clark, J. A., 1976. On post-glacial sea-level, *Geophys. J. R. astr. Soc.*, **46**, 647–667.

Forte, A. M. & Peltier, W. R., 1986. The inference of mantle viscosity from the flow induced by internal density heterogeneity, *J. geophys. Res.*, submitted.

Gilbert, F. & Dziewonski, A. M., 1975. An application of normal mode theory to the retrieval of structural parameters and source mechanisms from seismic spectra, *Phil. Trans. R. Soc. A*, **276**, 187–269.

Hager, B. H., 1984. Subducted slabs and the geoid: constraints on mantle rheology and flow, *J. geophys. Res.*, **89**, 6003–6015.

Haskell, N. A., 1935. The motion of a viscous fluid under a surface load. 1, *Physics* (N.Y.), **6**, 265–269.

Haskell, N. A., 1936. The motion of a viscous fluid under a surface load. 2, *Physics* (N.Y.), **7**, 56–61.

Hyde, W. T. & Peltier, W. R., 1985. Sensitivity experiments with a model of the ice age cycle: the response to harmonic forcing, *J. atmos. Sci.*, **42**, 2170–2188.

Jeffreys, H., 1972. Creep in the earth and planets, *Tectonophys.*, **13**, 569–581.

Lambeck, K., 1980. *The Earth's Variable Rotation: Geophysical Causes and Consequences*, Cambridge University Press, London.

Mareschal, J.-C. & Gangi, A., 1977. Equilibrium position of phase boundary under horizontally varying surface loads, *Geophys. J. R. astr. Soc.*, **49**, 757–772.

Masters, G., Jordan, T. H., Silver, P. G. & Gilbert, F., 1982. Aspherical earth structure from fundamental spheroidal-mode data, *Nature*, **298**, 604–613.

Minster, J. B., 1978a. Transient and impulses responses of a one dimensional linearly attenuating medium – I. Analytical results, *Geophys. J. R. astr. Soc.*, **52**, 479–501.

Minster, J. B., 1978b. Transient and impulse responses of a one dimensional linearly attenuating medium – II. A parametric study, *Geophys. J. R. astr. Soc.*, **52**, 503–524.

Muller, P. M. & Stephenson, F. R., 1975. The acceleration of the Earth and Moon from early astronomical observations, in *Growth Rhythms and History of the Earth's Rotation*, pp. 459–534, eds Rosenberg, G. D. & Runcorn, S. K., Wiley, New York.

Munk, W. H. & MacDonald, G. J. F., 1960. *The Rotation of the Earth*, Cambridge University Press.

Munk, W. H. & Revelle, R., 1952. On the geophysical interpretation of irregularities in the rotation of the Earth, *Mon. Not. R. astr. Soc., Geophys. Suppl.*, **6**, 331–347.

Nakiboglu, S. M. & Lambeck, K., 1980. Deglaciation effects upon the rotation of the Earth, *Geophys. J. R. astr. Soc.*, **62**, 49–58.

Nakiboglu, S. M. & Lambeck, R., 1981. Corrections to 'Deglaciation effects upon the rotation of the Earth', *Geophys. J. R. astr. Soc.*, **64**, 559.

O'Connell, R. J., 1976. The effects of mantle phase changes on postglacial rebound, *J. geophys. Res.*, **81**, 971–974.

Peltier, W. R., 1974. The impulse response of a Maxwell Earth, *Rev. Geophys. Space Phys.*, **12**, 649–669.

Peltier, W. R., 1976. Glacial isostatic adjustment II. The inverse problem, *Geophys. J. R. astr. Soc.*, **46**, 669–706.

Peltier, W. R., 1980. Mantle convection and viscosity, in *Physics of The Earth's Interior*, Proceedings of the International School of Physics 'Enrico Fermi', pp. 362–427, eds Dziewonski, A. M. & Boschi, E., North Holland, Amsterdam, New York.

Peltier, W. R., 1981. Ice age geodynamics, *Ann. Rev. Earth planet. Sci.*, **9**, 199–225.

Peltier, W. R., 1982. Dynamics of the Ice Age Earth, *Adv. Geophys.*, **24**, 1–146.

Peltier, W. R., 1983. Constraint on deep mantle viscosity from *LAGEOS* acceleration data, *Nature*, **304**, 434–436.

Peltier, W. R., 1984a. The rheology of the planetary interior, *Rheology*, **28**, 665–697.

Peltier, W. R., 1984b. The thickness of the continental lithosphere, *J. geophys. Res.*, **89**, 11 303–11 316.

Peltier, W. R., 1985a. Mantle convection and viscoelasticity, *Ann. Rev. Fluid. Mech.*, **17**, 561–608.

Peltier, W. R., 1985b. The *LAGEOS* constraint on deep mantle viscosity: results from a new normal mode method for the inversion of viscoelastic relaxation spectra, *J. geophys. Res.*, **90**, 9411–9421.

Peltier, W. R., 1986. Deglaciation induced vertical motion of the North American continent and transient lower mantle rheology, *J. geophys. Res.*, in press.

Peltier, W. R. & Andrews, J. T., 1976. Glacial isostatic adjustment I: the forward problem, *Geophys. J. R. astr. Soc.*, **46**, 605–646.

Peltier, W. R., Farrell, W. E. & Clark, J. A., 1978. Glacial isostasy and relative sea level: a global finite element model, *Tectonophys.*, **50**, 81–110.

Peltier, W. R. & Hyde, W. T., 1984. A model of the ice age cycle, in *Milankovitch and Climate vol. III*, pp. 565–580, eds Berger, A., Imbrie, J., Hays, J., Kukla, G. & Saltzman, B., Reidel, Dordrecht.

Peltier, W. R. & Wu, P., 1982. Mantle phase transitions and the free air gravity anomalies over Fennoscandia and Laurentia, *Geophys. Res. Lett.*, **9**, 731–734.

Peltier, W. R. & Wu, P., 1983. Continental lithospheric thickness and deglaciation induced true polar wander, *Geophys. Res. Lett.*, **10**, 181–184.

Peltier, W. R., Wu, P. & Yuen, D. A., 1981. The viscosities of the planetary mantle, in *Anelasticity in the Earth*, eds Stacey, F. D., Nicholas, A. & Paterson, M. S., American Geophysical Union, Washington, DC.

Quinlan, G. & Beaumont, C., 1984. Appalachian thrusting, lithospheric flexure and the Paleozoic stratigraphy of the Eastern interior of North America, *Can. J. Earth Sci.*, **21**, 973–996.

Richards, M. A. & Hager, B. H., 1984. Geoid anomalies in a dynamic Earth, *J. geophys. Res.*, **89**, 5987–6002.

Rubincam, D. P., 1984. Postglacial rebound observed by *LAGEOS* and the effective viscosity of the lower mantle, *J. geophys. Res.*, **89**, 1077–1087.

Sabadini, R. & Peltier, W. R., 1981. Pleistocene deglaciation and the Earth's rotation: implications for mantle viscosity, *Geophys. J. R. astr. Soc.*, **66**, 552–578.

Sammis, C. G., Smith, J. C., Schubert, G. & Yuen, D. A., 1977. Viscosity-depth profile of the Earth's mantle: effects of polymorphic phase transitions, *J. geophys. Res.*, **82**, 3747–3761.

Vincente, R. O. & Yumi, S., 1969. Co-ordinates of the pole (1899–1968) returned to the conventional international origin. *Publ. int. Latit. Obs. Mizusawa*, **7**, 41–50.

Vincente, R. O. & Yumi, S., 1970. Revised values (1941–1961) of the co-ordinates of the pole referred to the CIO, *Publ. int. Latit. Obs. Mizusawa*, 7, 109–112.

Walcott, R. I., 1970. Flexural rigidity, thickness and viscosity of the lithosphere, *J. geophys. Res.*, 75, 3941–3954.

Weertman, J., 1978. Creep laws for the mantle of the Earth, *Phil. Trans. R. Soc. A*, **288**, 9–26.

Wolf, Detlef, 1985. The normal modes of a layered incompressible Maxwell half space, *J. Geophys.*, 57, 106–117.

Woodhouse, J. H. & Dziewonski, A. M., 1984. Mapping the upper mantle: three dimensional modelling of earth structure by inversion of seismic waveforms, *J. geophys. Res.*, **89**, 5953–5986.

Wu, P. & Peltier, W. R., 1982. Viscous gravitational relaxation, *Geophys. J. R. astr. Soc.*, **70**, 435–486.

Wu, P. & Peltier, W. R., 1983. Glacial isostatic adjustment and the free air gravity anomaly as a constraint on deep mantle viscosity, *Geophys. J. R. astr. Soc.*, **74**, 377–449.

Wu, P. & Peltier, W. R., 1984. Pleistocene deglaciation and the Earth's rotation: a new analysis, *Geophys. J. R. astr. Soc.*, **76**, 753–592.

Yoder, C. F., Williams, J. G., Dickey, J. O., Schultz, B. E., Eanes, R. J. & Tapley, B. D., 1983. Secular variation of Earth's gravitational harmonic J_2 coefficient from Lageos and nontidal acceleration of earth rotation, *Nature*, **303**, 757–762.

Yuen, D. A. & Peltier, W. R., 1982. Normal modes of the viscoelastic earth, *Geophys. J. R. astr. Soc.*, 69, 495–526.

Zumberge, M. A., Faller, J. E. & Gschwind, J., 1983. Results from an absolute gravity survey in the United States, *J. geophys. Res.*, **88**, 7495–7502.

Zumberge, M. A., Rinkler, R. L. & Faller, J. E., 1982. A portable apparatus for absolute measurements of the Earth's gravity, *Metrologia*, **18**, 145–152.